HOT ELECTRON EFFECT IN ULTRATHIN PHOTOVOLTAIC DEVICES

A Thesis
Submitted to the Graduate Faculty
of the
North Dakota State University
of Agriculture and Applied Science

By

Deyan Ivov Mihaylov

In Partial Fulfillment
for the Degree of
MASTER OF SCIENCE

Major Department:
Physics

June 2012

Fargo, North Dakota

North Dakota State University

Graduate School

Title

HOT ELECTRON EFFECT IN ULTRATHIN PHOTOVOLTAIC DEVICES

By

Deyan Ivov Mihaylov

The Supervisory Committee certifies that this *disquisition* complies with North Dakota
State University's regulations and meets the accepted standards for the degree of

MASTER OF SCIENCE

SUPERVISORY COMMITTEE:

Val Marinov
Chair

Erik Hobbie

Orven Swenson

Ivan Lima

Approved by Department Chair:

06/14/2012   Daniel Kroll
Date   Department Chair

ABSTRACT

The focus of the research work described in the following thesis is increasing the efficiency of photovoltaic devices by reducing hot carrier thermalization losses. In principle this can be achieved by reducing the size of the absorber down to lengths comparable to the thermalization length for hot carriers. With the use of ultrathin absorbers hot carrier can be collected before they have reached thermal equilibrium with the lattice. The theoretical work on the subject is comprised of improving the empirical relationship developed in the most recent publication on the topic by. By making the assumption that the energy loss rate fits the exponential decay model, an expression for the energy as a function of absorber thickness was developed. The experimental work consist of fabricating devices with different absorber thicknesses and testing their ability to show change in performance due to collection of hot electrons.

ACKNOWLEDGMENTS

DEDICATION

I would like to dedicate this work to my parents, Ivo Mihaylov and Veneta Mihaylova, for always making my education a priority in mine and their lives.

TABLE OF CONTENTS

vii

LIST OF TABLES

LIST OF FIGURES

x

LIST OF SYMBOLS

A .... cross sectional area of p-n junction

D .... diffusion coefficient

d_{abs} .... absorber thickness

E .... energy

E_b .... bandgap energy

E_c .... energy of the lowest level of the conduction band

E_{cn} .... energy of the lowest level of the conduction band in n-doped material

E_{cp} .... energy of the lowest level of the conduction band in p-doped material

E_F .... energy of the Fermi level

E_{Fn}............... quasi-Fermi level for electrons

E_{Fp}............... quasi-Fermi level for holes

E_i .... initial energy of a hot carrier immediately after excitation

E_v .... energy of the highest level of the valence band

E_{vn} .... energy of the lowest level of the valence band in n-doped material

E_{vp} .... energy of the lowest level of the valence band in p-doped material

$\mathcal{E}_0$ .... equilibrium electric field

$h, \hbar$............... Planck's constant (4.135×10^{-15}), reduced Plack's constant ($2\pi h$)

I_{sc} .... short circuit current

k_B .... Boltzmann's constant (8.617×10^{-5} eV K^{-1})

L_n .... Diffusion length for electrons

L_p .... Diffusion length for holes

n .... electron density in the conduction band

n_n .... majority carrier density on the n-side of a p-n junction

n_p .... minority carrier density on the p-side of a p-n junction

N_a .... acceptor density

N_d .... donor density

p .... hole density in the valence band

p_n .... minority carrier density on the n-side of a p-n junction

p_p .... majority carrier density on the p-side of a p-n junction

q .... elementary charge (1.602×10^{-16} C)

T .... temperature

U .... light intensity

V .... potential

V_0 .... contact potential across a p-n junction

V_f .... forward bias

V_n .... voltage potential on the n-side of a p-n junction

V_{oc} .... open-circuit voltage

V_p .... voltage potential on the p-side of a p-n junction

V_r .... reverse bias

W .... width of depletion region

x_n .... penetration of depletion region on the n-side of a p-n junction

x_p .... penetration of depletion region on the p-side of a p-n junction

x_{n0} .... penetration of depletion region on the n-side of a p-n junction in equilibrium

x_{p0} .... penetration of depletion region on the p-side of a p-n junction in equilibrium

γ .... collision rate

δn .... excess electrons

Δn_p............... excess electrons at edge of depletion region on the p-side (cm^{-3})

δp .... excess holes

Δp_n............... excess holes at edge of depletion region on the n-side (cm^{-3})

ϵ .... permittivity; $\epsilon_0 \epsilon_r$

ϵ_0 .... permittivity of free space

ϵ_r .... relative dielectric constant

μ .... electron mobility

ν .... frequency

ρ .... charge density

ϕ_S .... work function of semiconductor

ϕ_M .... work function of metal

χ .... electron affinity

ψ .... wave function

ω .... angular frequency of light

CHAPTER 1. INTRODUCTION

One of the main subjects in photovoltaic technology research is utilizing as much of the energy of the solar spectrum as possible. Light incident upon the Earth is composed of photons of a wide range of frequencies. The spectrum spans frequencies ranging from deep UV to far infra-red. However, light of frequencies spanning the visible range is of considerably higher intensity than the rest of the spectrum. Figure 1 below shows the intensity of light emitted by the sun as a function of wavelength ($\propto$ 1/frequency).

Our Sun's Spectrum
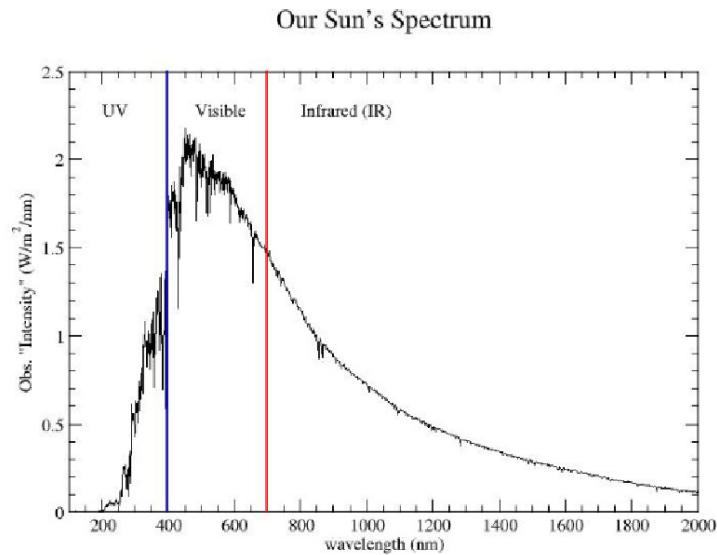
Figure 1. *Blackbody radiation curve for our sun: The highest intensity corresponds to frequencies in the visible range*[1].

Although the Earth's surface is illuminated by a broad range of frequencies, the conventional photovoltaic device cannot make use of the entire solar spectrum. In order to convert light into electricity, the energy of the incoming light has to be above a certain threshold. For electrical current to be generated, electrons in semiconducting materials comprising the photovoltaic device need to be freed (excited from the

valence band into the conduction band) from the atoms. For different semconductors, the energies of excitation have different minimum values since different semiconductors have different bandgaps, which is the required energy to excite a charge carrier from the valence band where it is bound to the atom, into the conduction band where it is free to move. According to Einstein's equation $E = \hbar\omega$, where $\hbar$ is the reduced Planck's constant and $\omega = 2\pi\nu$, the frequency (ν) of light is directly proportional to E [2]. Fig. 2 below illustrates how light of insufficient energy is not being utilized by the solar cell.
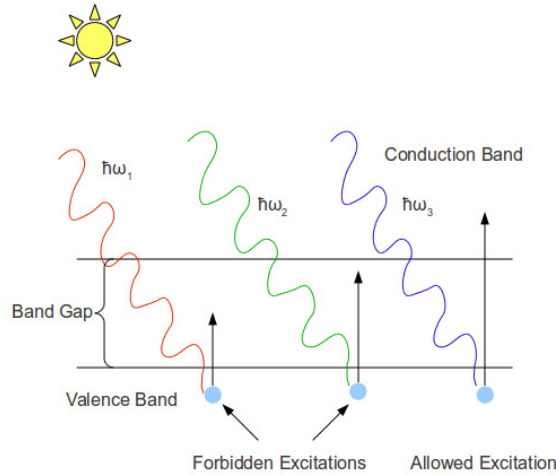
Figure 2. *Allowed and forbidden excitations: Three photons of arbitrary energies $\hbar\omega_1 < \hbar\omega_2 < \hbar\omega_3$ being absorbed by electrons. The photons of energies $\hbar\omega_1$ and $\hbar\omega_2$ are not energetic enough to excite electrons into the conduction band and therefore, are not absorbed. The photon of energy ω_3, however is energetic enough to excite an electron into the conduction band and it's energy can be utilized [2].*

Photons of energies well above the bandgap excite electrons to energy states a lot higher than the bottom of the conduction band. The lifetimes of those states are many orders of magnitude shorter than the lifetime of the lowest energy state in the conduction band [3]. As a result, highly energetic (hot) electrons quickly lose their extra energy in a process known as thermalization and fall to the bottom of the

conduction band where they spend most of their lifetime before they either return back to the valence band or are collected as current. The mechanics of collecting photoexcited electrons as current are described in detail in later chapters. Here, it is important to note that the bandgap of the absorbing material is what determines what portion of the energy of light is utilized. Fig. 3 below illustrates the process of thermalization [4].
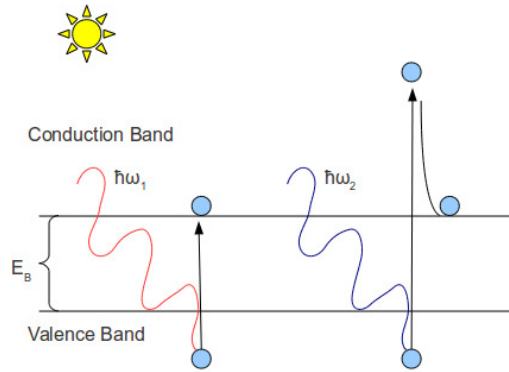
Figure 3. *Excitation and thermalization: An electron excited to the bottom of the conduction band by a low-energy red photon $\hbar\omega_1$ and a hot electron excited well above the bottom of the conduction band by a high-energy blue photon $\hbar\omega_2$. The hot electron loses its extra energy in a process known as thermalization. The time it takes a hot electron to thermalize to the bottom of the conduction band depends on the material, however reported values vary from 0.1 to 10* ps[4, 3]

Fig. 3 above represents what is known as the 'spectrum losses' part of the Shockley-Queisser limit [5]. The Shockley-Queisser limit is a theoretical limit on the efficiency of solar cells calculated based on three major loss mechanisms:

Spectrum losses: These losses are defined in terms of two processes - 1) photons of energy $E < E_B$, where E_B is the bandgap energy of the absorbing material, cannot excite electrons into the conduction band and their energy is converted to thermal energy and 2) photons of energy $E > E_B$ excite electrons well above the bandgap, which then thermalize to the bottom of the conduction band, thus

converting the excess light energy into thermal energy. The first process lowers the efficiency limit by about 20 % depending on the size of the bandgap and the second process by an additional 30 %, making spectrum losses the most prominent factor in the Shockley-Queisser limit [6].

Recombination losses: As electrons are excited from the valence into the conduction band they leave a positive charge on the atom they were excited from. The positive charge is referred to as a 'hole' and it moves through the material in a manner similar to an electron. Holes, however, are much slower than excited electrons, thus taking longer to diffuse to the electrode. When an excited electron collides with the hole of a previously excited electron the two recombine and are never utilized as current. Recombination losses account for another 10 % of the limit [6].

Blackbody radiation losses: Photovoltaic devices usually operate at temperatures around 300 K which makes them emit blackbody radiation which cannot be utilized. This loss mechanism brings the limit on efficiency down approximately another 7 % [6].

Since spectrum losses represent the major factor in the Shockley-Queisser limit, modern day photovoltaic research is aimed at minimizing those losses. Recent advances in utilizing the high-energy part of the solar spectrum were reported in a 2009 paper titled "Hot electron effect in nanoscopically thin photovoltaic junctions" by Kempa *et al.* in which the authors reported a *p-i-n* junction solar cell with an ultra-thin absorber which exhibited a higher open-circuit voltage when illuminated by light of higher frequency [7]. Fig. 4 below shows the *I-V* curve obtained.

The method for collecting hot electrons suggested by Kempa and co-workers is based on the fact that even though the time for thermalization is very small, it is still
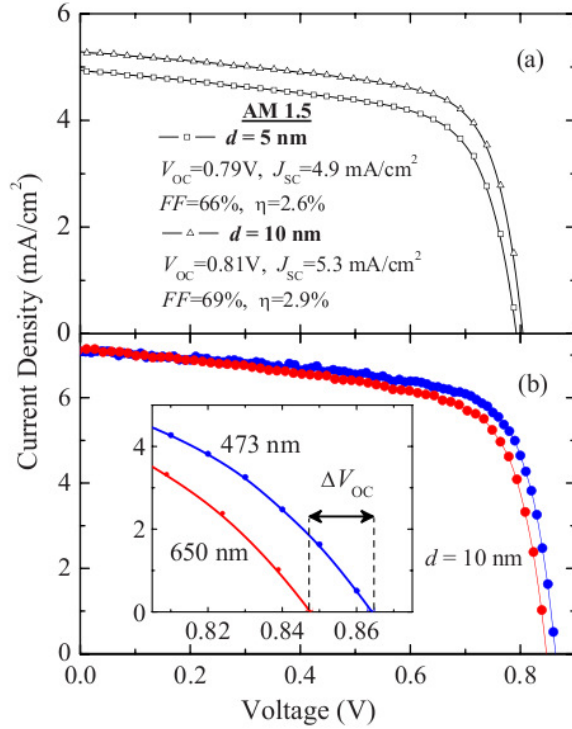
Figure 4. *The Current-Voltage (I-V) characteristics for the ultra-thin absorber a-Si device fabricated by Kempa et al: The graph above represents the difference in performance by two cells of different absorber layer thickness. The bottom graph shows the difference in open-circuit voltage produced by a device with absorber layer thickness of 10 nm when irradiated by red and blue laser light [7].*

of some finite value, during which the electron drifts towards the edge of the absorber region where it is collected as current. Therefore, if the absorber thickness is smaller than the drift length of the hot electron, then that electron can be collected before it has thermalized to the bottom of the conduction band. The following thesis presents a semi-classical theory on the dynamics of hot electron thermalization, a detailed analysis on the results obtained by Kempa *et al.* and experimental work aiming to replicate their results using semiconductors with crystalline structure.

The dynamics of charge carriers in semiconductors is what lies behind the principles of photovoltaic conversion. The following sections deal with the statistical mechanics of an electron gas.

2.1. The Electron Gas

The physical properties of an electron gas are important in analyzing the electrical properties of semiconductors since the electrons responsible for current are free to move throughout the lattice. The analysis the electron gas starts with considering the ground state properties of a system of N electrons confined to a volume V. Furthermore, interactions between particles are neglected. Therefore, the only restriction applied on the system is that the particles have to abide by the rules of the Pauli exclusion principle, which states that no two identical fermions (such as electrons) can occupy the same energy level. Since the electrons are non-interacting, the energy levels for the system of N electrons are the same as if there were one electron confined within the same volume. At T=0, this electron will occupy the lowest energy level and every additional electron added to the system will occupy the next lowest energy level available. Of course, this treatment of the electron gas is only possible of the energy levels are quantized and not continuous. The energy spectrum of a single electron confined in a volume V can be determined by solving the time independent Schrödinger equation

$$-\frac{\hbar^2}{2m}\nabla\psi(\mathbf{r}) + V(\mathbf{r})\psi(\mathbf{r}) = E\psi(\mathbf{r}) \tag{1}$$

The geometircal shape that simplifies the mathematics is a cube with of side L within which the wave function of the electron is subject to the following bound-

ary conditions[13]

$$\psi(x, y, z + L) = \psi(x, y, z) \tag{2a}$$

$$\psi(x, y + L, z) = \psi(x, y, z) \tag{2b}$$

$$\psi(x + L, y, z) = \psi(x, y, z) \tag{2c}$$

Eq. 2 is also known as the Born-von Karman periodic boundary condition and it's advantage is that it eliminates the potential at the walls while allowing for the number of particles within thus reducing the Schrödinger equation equation to

$$-\frac{\hbar^2}{2m}\nabla\psi(\mathbf{r}) = E\psi(\mathbf{r}) \tag{3}$$

The solution to Eq. 3 has the following form

$$\psi(\mathbf{r}) = \frac{1}{\sqrt{V}}e^{i\mathbf{k}\cdot\mathbf{r}} \tag{4}$$

where $\mathbf{k}$ is the wave vector of the plane wave $e^{i\mathbf{k}\cdot\mathbf{r}}$. The energy of the electron can be expressed in terms of $\mathbf{k}$ according to

$$E(\mathbf{k}) = \frac{\hbar^2 k^2}{2m} \tag{5}$$

The wave vector $\mathbf{k}$ can be directly related to the momentum of the particle. The quantum mechanical momentum operator is [8]

$$\mathbf{p} = \frac{\hbar}{i}\frac{\partial}{\partial\mathbf{r}} \tag{6}$$

and when applied on $e^{i\mathbf{k}\cdot\mathbf{r}}$, which is an eigenstate of the operator, the following is

obtained

$$\mathbf{p} = \hbar\mathbf{k} \tag{7}$$

from which the velocity ($\mathbf{v}=\mathbf{p}/$m) can be expressed as

$$\mathbf{v} = \frac{\hbar\mathbf{k}}{m} \tag{8}$$

Combining Eqs. 5 and 8, the energy of the particle can be expressed as

$$E = \frac{1}{2}mv^2 \tag{9}$$

An important property of the electron is that it can only take on certain values of energy. This is a result of the fact that $\mathbf{k}$ can only take on certain values allowed by the boundary condition. Combining Eqs. 2 and 4 the following relationship is obtained

$$e^{ik_x L} = e^{ik_y L} = e^{ik_z L} = 1 \tag{10}$$

which restricts the allowed values of $\mathbf{k}$ to integer multiples of $2\pi/L$ since $e^x = 1$ only for $x = 2\pi i n$ where n is an integer. Therefore, the energy states of an electron are in fact quantized. Since k is quantized in all three space directions x, y and z, it is customary to map the discrete k values in what is know as k-space. k-space is a three dimensional space with axes corresponding to k_x, k_y and k_z as shown in Fig. 5 below Now that the energy spectrum is determined, the ground state energy configuration of the electrons in the gas can also be determined. Adhering to the Pauli exclusion principle, the energy state in center of the coordinate system in Fig. 5 is filled first with two electrons, next the six neighboring states corresponding to $k_x = \pm 2\pi/L$, $k_y = \pm 2\pi/L$ and $k_z = \pm 2\pi/L$ are filled with 12 electrons and so on. In the limit of many electrons k-space is a sphere of constant radius k_F known as the Fermi-radius.
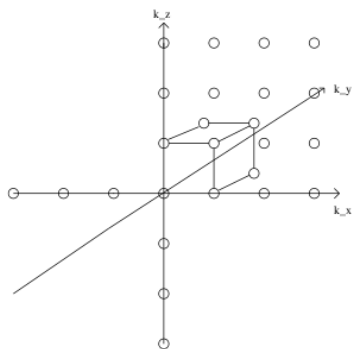
Figure 5. *k-space: Allowed values of* **k** *in k-space are represented by individual nodes* [2]

Consequently, the energy corresponding to k_F can be defined through Eq. 5.

$$E_F = \frac{\hbar^2 k_F^2}{2m} \tag{11}$$

An important property is the total energy of the electron gas, which can be expressed in terms of the Fermi-energy in Eq. 11. The total energy is the sum of the energies of all electrons within the k-sphere[13]

$$\sum_{\mathbf{k}} E = 2 \underbrace{\frac{V}{8\pi^3}}_{\text{number of states per unit volume}} \int_0^{k_F} \overbrace{\left[4\pi k^2 \frac{\hbar^2 k^2}{2m} \right]}^{\text{volume of k-shpere times energy of each electron}} \mathrm{d}k \tag{12}$$

which gives

$$\sum_{\mathbf{k}} E = E_{tot} = \frac{V}{\pi^2} \frac{\hbar^2 k_F^5}{10m} \tag{13}$$

Dividing by the number of electrons in the k-sphere the energy per electron can be obtained. The total number of electrons in the sphere is the volume of the sphere

9

×the density of levels ×the number of electrons available per level

$$N = 2\left(\frac{4\pi k_F^3}{3}\right)\left(\frac{V}{8\pi^3}\right) = \frac{k_F^3}{3\pi^2}V \tag{14}$$

Dividing Eq. 13 by Eq. 14 an expression for the average energy in the electron gas is obtained

$$\frac{E_{tot}}{N} = \frac{3}{5}E_F \tag{15}$$

Eq. 15 was obtained for the case of $T = 0$. However, at $T > 0$ the average energy should increase since the average kinetic energy of the electrons is increased. In order to determine the temperature dependence of the total energy for a fermion gas, Eq. 12 needs to be corrected with by factoring in the probability of each state being occupied as a function of temperature. This probability is given by the Fermi-Dirac distribution function[9]

$$F(E) = \frac{1}{\exp(E - E_F)/k_B T + 1} \tag{16}$$

After changing variables from k to E according to $k = \sqrt{2mE/\hbar^2}$ an integral of the following form is obtained

$$E_{tot} = [const.] \int_0^\infty E^2 F(E) \mathrm{d}E \tag{17}$$

which has a solution of the form [10]

$$E = \frac{3}{5}NE_F\left[1 + \left(\frac{5\pi^2}{12}\right)\left(\frac{k_B T}{E_F}\right)^2\right] \tag{18}$$

10

2.2. Band Structure

In studying the physical properties of solids the most important piece of information is the arrangement of the allowed energy states of the electrons. The energy states of a quantum particle in a certain potential are described by the Schrödinger equation[11]

$$-\frac{\hbar^2}{2m}\frac{d^2\psi}{dx^2} + V(x)\psi = E\psi \tag{19}$$

In the case of solids, the quantum particle (the electron) is confined by a periodic potential represented by the stationary, positively charged and evenly spaced nuclei. In the relatively vast space between the nuclei the potential is zero but as the particle approaches a nucleus the potential spikes up. Therefore, if the potential induced by each nucleus can be approximated by a delta function positioned at the nucleus. The electron in the solid would experience a potential of the following form

$$V(x) = -\alpha \sum_{j=0}^{N-1} \delta(x - ja) \tag{20}$$

where N is on the order of Avogadro's number, α represents the strength of the potential and a is the spacing between adjacent delta functions. Solving the Schrödinger equation for the region $0 < x < a$ where the potential is zero, applying Bloch's theorem

$$\psi(x + a) = e^{iKa}\psi(x) \tag{21}$$

and applying the boundary conditions that ψ is continuous everywhere and $d\psi/dx$ is discontinuous only where the potential is infinite, the following relation is obtained

$$\cos(\mathbf{K}a) = \cos(ka) + \frac{m\alpha}{\hbar^2 k}\sin(ka) \tag{22}$$

where $\mathbf{K}$ is a real and independent of x constant which represents the reciprocal

lattice vector of a lattice with a certain periodicity and $k = \sqrt{2mE/\hbar^2}$ is the wave vector of a plane wave traveling through the lattice. Figure 6 shows the right side, $f(ka) = \cos(ka) + \frac{m\alpha}{\hbar^2 k}\sin(ka)$, of the equation plotted vs ka as well as the limits of the function $F(\mathbf{K}a) = \cos(\mathbf{K}a)$.

Figure 6. *Sinc function representing allowed and forbidden energy bands in solid state materials: The function $f(ka) = \cos(ka) + \frac{m\alpha}{\hbar^2 k}\sin(ka)$ plotted vs ka along with the limits of the function $F(\mathbf{K}a) = \cos(\mathbf{K}a)$ which spans the domain between -1 and 1.* [11]

For every value of $f(ka)$ within the domain $[-1, 1]$ there exists an allowed energy state. Since $f(ka)$ has an infinite set of values within the domain $[-1, 1]$ there are infinitely many energy states in the range of $f(ka)$ corresponding to that domain. Hence, for the range of values of $f(ka)$ that "spill over" the allowed domain, a bandgap is formed [11].

2.3. Direct vs Indirect Bandgap

Considering the case for free electrons i.e. $\alpha = 0$ and implementing the periodicity of the cosine function in 2π Eq. 22 can be written

$$\cos(ka) = \cos(K_x a + n2\pi), \qquad n = 0, \pm 1, \pm 2, ... \tag{23}$$

where K_x is the wave vector $\mathbf{K}$ in one dimension. Therefore, an expression for K_x

can be derived, which takes the following form

$$K_x = \sqrt{\frac{2m}{\hbar^2}}E^{1/2} - n\frac{2\pi}{a}, \qquad n = 0, \pm 1, \pm 2, ... \tag{24}$$

or after solving for E,

$$E = \frac{\hbar^2}{2m}\left(K_x + n\frac{2\pi}{a}\right)^2, \qquad n = 0, \pm 1, \pm 2, ... \tag{25}$$

This model gives the shape of the energy bands in k-space of a free electron traveling in a periodic lattice along the x direction. However, in order to obtain the energy band diagram for a three-dimansional crystal all possible paths that an electron could take need to be taken into account. For that purpose, the terms inside the brackets of eq. 25 need to become vectors. As a result

$$E = \frac{\hbar^2}{2m}\left(\mathbf{k} + \mathbf{G}\right)^2, \tag{26}$$

where $\mathbf{G}$ is called the translation vector and it depends on the atomic structure of the crystal. Different types of lattices (simple cubic, body centered cubic, face centered cubic etc.) have radically different translation vectors and therefore different band diagrams. Other essential factors involved in determining the band structure of materials is the spacing between adjacent atoms and their atomic mass since the effective mass of the electron depends on the spacing between potential barriers as well as on their strength [12, 13].

Regardless of the complexity of the energy band structure of different semiconductors used in the manufacturing of photovoltaic devices, there are two types of bandgaps: direct or indirect. A direct bandgap is established when the maximum of the valence band matches the minimum of the conduction band in k-space i.e. they

13

occur at the same value for $\mathbf{k}$. Conversely, indirect bandgaps occur when the maximum of the valence band and the minimum of the conduction band occur at different values for $\mathbf{k}$ [4]. In the case of a direct bandgap an excitation from the valence band into the conduction band is achieved via a photon of energy $E_c - E_v$ where E_c is the energy of the bottom of the conduction band and E_v is the energy of the top of the valence band. On the other hand, in the case of an indirect bandgap a photon of energy $E_c - E_b$ alone is not enough to cause an excitation. It needs to be accompanied by a phonon of momentum $\mathbf{k}_c - \mathbf{k}_v$ where $\mathbf{k}_c$ is the crystal momentum at which the bottom of the conduction band occurs and $\mathbf{k}_v$ is the crystal momentum at which the top of the valence band occurs. Fig. 7 below shows the energy bands in k-space and the difference in electronic transitions from the valence band to the conduction band [13, 14].
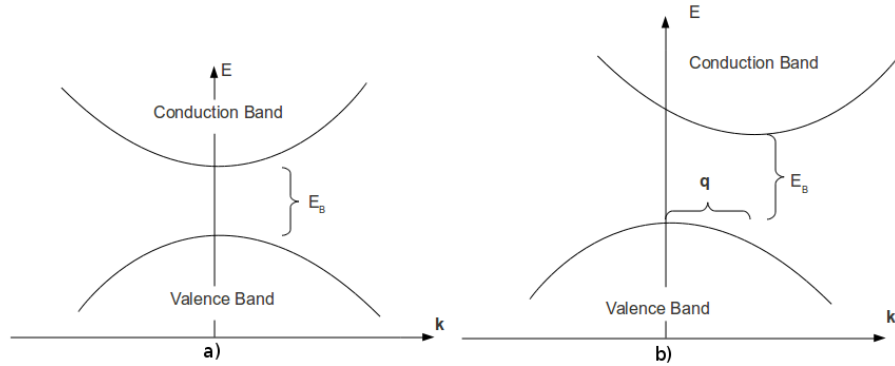

Figure 7. *Direct and indirect bandgap: a) Direct bandgap. An excitation from the valence band into the conduction band can be achieved through absorption of a photon of energy $E_B = \hbar\omega$. b) Indirect bandgap. Exciting an electron from the valence into the conduction band requires not only absorption of a photon of energy $E_B = \hbar\omega$ but also absorption of a phonon of momentum $\hbar\omega(\mathbf{q})$ where $\mathbf{q}$ is a vector in k-space corresponding to the mismatch between the bottom of the conduction band and the top of the valence band. [13]*

14

2.4. The *p-n* Junction

Solar energy conversion is only possible if charge separation is achieved. All solar energy conversion technologies employ the *p-n* junction as means for charge separation. The following sections aim at explaining how the *p-n* junction, or a version of it (the *p-i-n* junction), is built and how it operates, which is important information employed in theoretical and experimental research developed in later chapters

2.4.1. Extrinsic Semiconductors

Introducing impurities into an intrinsic semiconductor, a process also known as *doping*, has a significant effect on the conductivity of the material since the impurities introduce charge carriers. Doping a semiconductor with impurity atoms that cause a shift in the Fermi-level up is called *n*-doping and conversely, doping a semiconductor with impurities that shift the Fermi-level down is called *p*-doping. Thus, an extrinsic semiconductor has an equilibrium carrier density n_0 or p_0 different from the carrier density present prior to doping. Elements used for *n*-doping are column *V* elements such as P, As and Sb. These elements introduce an energy level close to the conduction band, which at 0 K is full of electrons. However, this energy level is so close to the conduction band that at slightly higher temperatures (300 K) nearly all the electrons are donated to the conduction band through thermal excitation. Therefore, column *V* elements are known as donor impurities and materials doped with donor impurities are known as *n*-type materials. On the other hand, column III elements like B, Al, Ga and In introduce an energy level close to the valence band which at 0 K is empty. In a manner similar to *n*-doping these levels are filled with electrons at higher temperatures, which partially fills the valence band with holes (which act as positive charges). Therefore these elements are known as acceptor impurities [15].

2.4.2. Contact Potential

Considering the fact that no net current flows across a p-n junction at equilibrium, the drift current must be of equal magnitude and opposite direction of the diffusion current. This, combined with the fact that there is no net build up of charge on either side of the junction gives :

$$J_{p(drift)} + J_{p(diffusion)} = 0 \tag{27}$$

$$J_{n(drift)} + J_{n(diffusion)} = 0 \tag{28}$$

where J represents the current density through the junction [15]. The gradient in the electrostatic potential across the depletion region W is in a direction opposite to the direction of the electric field $\mathcal{E}$. The relationship between the electrostatic potential V and the electric field is well known [8]:

$$\mathcal{E}(x) = -\frac{dV(x)}{dx}$$

Thus, under the assumption that the electric field in the neutral n and the neutral p regions is zero, and therefore the potentials V_n and V_p are also constant, a potential difference (contact potential)

$$V_o = V_n - V_p \tag{29}$$

can be defined [15]. This difference in contact potential separates the energy bands as shown in Fig. 8 so that at equilibrium the Fermi level is constant throughout the device.

It is of interest to relate the contact potential to the electron and hole densities on either side of the junction. This can be done by considering Eq. 27 and defining
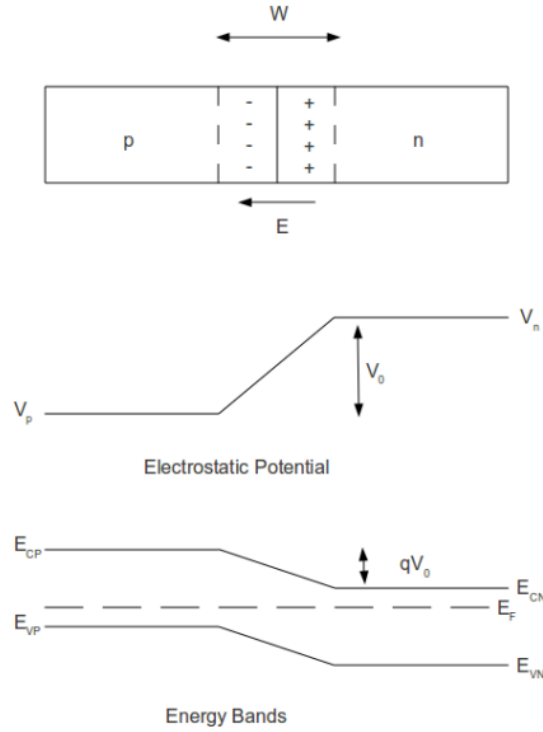
Figure 8. *p-n junction in equilibrium: A p-n junction showing the depletion region W, the electrostatic contact potential across the junction and the energy band diagram [15].*

the drift current density as

$$J_{p(drift)}(x) = q\mu_p p(x)\mathcal{E}(x) \tag{30}$$

where q is the elementary charge, μ_p is the hole mobility, and $p(x)$ is the hole density in the conduction band. The diffusion current is defined as

$$J_{p(diff)}(x) = qD_p\frac{dp(x)}{dx} \tag{31}$$

where D_p is the diffusion coefficient for holes defined by the Einstein relation $\frac{D}{\mu} = \frac{k_B T}{q}$

where k_B is the Boltzmann constant. This gives the following equation

$$\frac{\mu_p}{D_p}\mathcal{E}(x) = \frac{1}{p(x)}\frac{dp(x)}{dx} \qquad (32)$$

Using the Einstein relation and expressing the electric field in terms of the gradient gives

$$-\frac{q}{k_BT}\frac{dV(x)}{dx} = \frac{1}{p(x)}\frac{dp(x)}{dx} \qquad (33)$$

Solving this differential equation by integration gives a relationship between the voltage potential on either side of the junction and the hole densities in the neutral regions just outside the transition regions:

$$-\frac{q}{k_BT}\int_{V_p}^{V_n} dV = \int_{p_p}^{p_n}\frac{1}{p}dp \qquad (34)$$

$$-\frac{q}{k_BT}(V_n - V_p) = ln\frac{p_n}{p_p} \qquad (35)$$

Therefore, V_0 can be expressed in terms of p_n (majority carrier density) and p_p (minority carrier density)

$$V_0 = \frac{k_BT}{q}ln\frac{p_p}{p_n} \qquad (36)$$

or,

$$\frac{p_p}{p_n} = \exp\left(\frac{qV_0}{k_BT}\right) \qquad (37)$$

and for electron densities[15]

$$\frac{n_n}{n_p} = \exp\left(\frac{qV_0}{k_BT}\right) \qquad (38)$$

An important point Eqs. 37 and 38 make is that the minority carrier densities just outside the depletion region on either side of the junction decrease exponentially with respect to the magnitude of the contact potential, V_0, since the majority carrier density can be approximated as being constant throughout the neutral regions, as

18

discussed later in Sec. 3.

2.4.3. The Depletion Region

The depletion region W is defined as the region around the junction formed by uncompensated donor and acceptor ions. It is safe to assume that this region is void of charge carriers since the electric field formed by the ions sweeps out any charge that diffuses into the region. Therefore, the charge density within each region can be approximated by only considering the donor and acceptor ions and can be expressed as

$$Q_- = qAx_{n0}N_d \tag{39}$$

where A is the cross sectional area of the junction, x_{n0} is the depth of the depletion region on the n-side of the junction and N_d is the density of donor ions. Consequently, for the p-side of the junction

$$Q_+ = qAx_{p0}N_a \tag{40}$$

Since prior to creating the $p - n$ junction the two materials are neutral, the principle of charge conservation can be applied, which leads to

$$qAx_{p0}N_a = qAx_{n0}N_d \tag{41}$$

where

$$x_{p0} + x_{n0} = W \tag{42}$$

Therefore, it is evident from 41 that at different doping densities the length at which the depletion region extends into each material is different. These penetration lengths can be expressed in terms of the doping densities and the contact potential by the

following relations[15, 16]

$$x_{p0} = \left\{ \frac{2\epsilon V_0}{q} \left[\frac{N_d}{N_a(N_a + N_d)} \right] \right\}^{1/2} \tag{43}$$

$$x_{n0} = \left\{ \frac{2\epsilon V_0}{q} \left[\frac{N_a}{N_d(N_a + N_d)} \right] \right\}^{1/2} \tag{44}$$

2.4.4. Forward Bias

Forward bias is defined as connecting the p-doped region to the positive lead on a battery and the n-doped region to the negative lead. Under forward bias the potential barrier is lowered because the electrostatic potential on the p side is raised, thus, the width of the depletion region also decreases. As a result of the lowering of the potential barrier, the difference in the energy bands is lowered by an amount qV_f and equilibrium Fermi level is separated into quasi-Fermi levels the difference between which is aslo exactly qV_f. Fig. 9 illustrates how the depletion width, electrostatic field and potential across the junction are altered in the presence of a forward bias [15, 16].
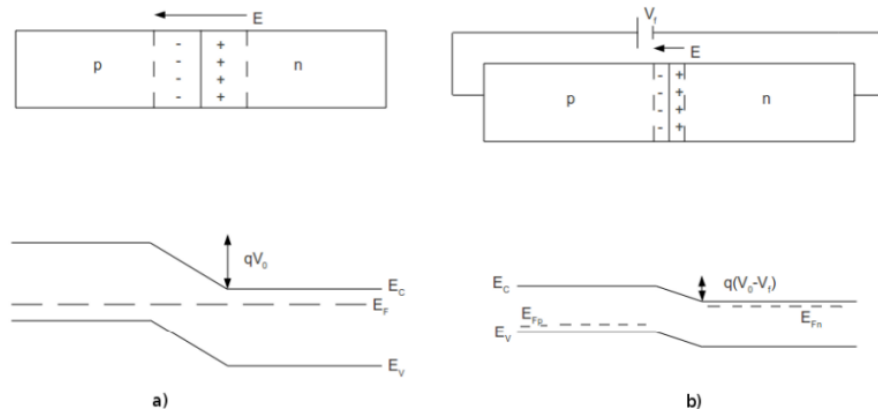

Figure 9. *The effect of forward bias on a p-n junction: a) Band diagram for a p-n junction in equilibrium. b) A forward bias lowers the potential barrier that charge carriers have to overcome. As a result the diffusion current overwhelms the drift current and charge flows through the circuit.*[15]

Quasi-Fermi levels appear on both sides of the junction because the electron and hole densities in the conduction and the valence band respectively change under applied bias. As electrons are injected into the conduction band on the n-side, the Fermi level for elecrons on the n-side is raised and similarly as holes are injected into the valence band on the p-side the Fermi level for holes on the p-side is lowered. The quasi-Fermi levels for electrons are defined in terms of the electron and hole densities via

$$E_{F_n} \equiv E_c + k_B T \ln\left(\frac{n}{N_c}\right) \tag{45a}$$

$$E_{F_c} \equiv E_v + k_B T \ln\left(\frac{p}{N_v}\right) \tag{45b}$$

Quasi-Fermi levels are important in the analysis of $p - n$ junctions because their difference corresponds to voltage applied across the junction according to $qV_f = E_{F_n} - E_{F_p}$. In other words, if one was to measure the voltage across a p-n junction the voltmeter would read $(E_{F_n} - E_{F_p})/q$ [17].

2.4.5. Reverse Bias

Reverse bias is defined as connecting the p-doped region to the *negative* lead and the n-doped region to the *positive* lead. In this situation, the electrostatic potential on the n side is raised which results in higher potential barrier between the two junctions. Consequently, at even small reverse voltages the diffusion current is eliminated. The drift current on the other hand, is independent of the height of the potential barrier since the minority carrier concentrations on either side of the junction are not affected by the applied voltage. Fig. 10 illustrates how applying a reverse potential across the p-n junction raises the potential barrier for majority carreir electrons but does not affect minority carrier drift current. In terms of quasi-Fermi levels, as electrons are injected into the p-side E_{F_p} is raised and as holes are injected into the n-side E_{F_n} is
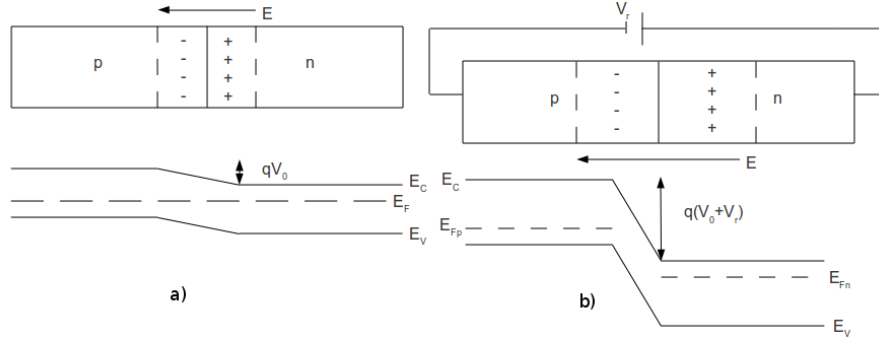
Figure 10. *The effect of reverse bias on a p-n junction: a) Band diagram for a p-n junction in equilibrium. b) A reverse bias raises the potential barreir that majority carrier electrons on the n side have to overcome thus eliminating the diffusion current.*[15]

lowered. As a result qV_r is negative and the overall potential across the junction is raised.

2.5. The *p-i-n* Junction

A *p-i-n* junction is formed when an undoped (intrinsic) region is sandwiched between a *p*-doped and an *n*-doped region. In this situation both electrons and holes diffuse into the intrinsic region, combine with each other and leave the intrinsic region uncharged. In equilibrium, it can be safely assumed that there is no charge density, ρ, in the intrinsic region i.e. $\rho(x) = 0$, therefore the electric field throughout the *i*-region can be taken as constant. Fig. 11 shows the approximate profile of the electric field thoughout the whole *p-i-n* junction. The electric field in the region containing charge can be approximated using Gauss's law [8]

$$\frac{d\mathcal{E}}{dx} = -\frac{\rho}{\epsilon} \tag{46}$$

and assuming the electric field outside the depletion region on the doped sides is zero. The charge density in the *p* region is $-qN_a$ and the charge density in the *n* region is qN_d. Using these charge densities and applying Eq. 46 the electric field can be
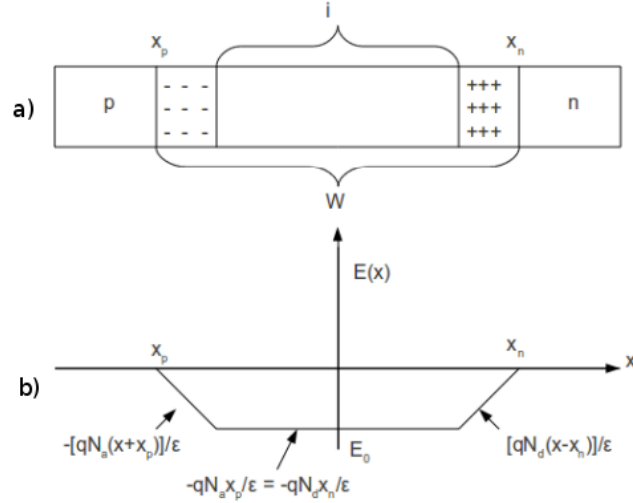
22

Figure 11. *The effect of forward bias on a p-i-n junction: a) Band diagram for a p-i-n junction in equilibrium. b) A reverse bias raises the potential barrier that majority carrier electrons on the n side have to overcome thus eliminating the diffusion current* [15].

approximated by integrating over the appropriate limits. This gives

$$\mathcal{E}(x) = -\frac{qN_a(x + x_p)}{\epsilon} \tag{47}$$

for the electric field just outside the intrinsic region on the *p*-side of the junction and

$$\mathcal{E}(x) = \frac{qN_d(x - x_n)}{\epsilon} \tag{48}$$

for the electric field just outside the intrinsic region on the *n*-side of the junction. The electric field throughout the *i*-region is constant and its value is the maximum value that the electric field across the junction reaches. Its value is obtained by solving

$$\frac{d\mathcal{E}}{dx} = \frac{q}{\epsilon}N_d \qquad 0 < x < x_{n0} \tag{49}$$

23

or

$$\frac{d\mathcal{E}}{dx} = \frac{q}{\epsilon} N_a \qquad -x_{p0} < x < 0 \tag{50}$$

for $\mathcal{E}_0$. The solution to differential Eqs. 49 and 50 provides the following expression

$$\mathcal{E}_0 = -\frac{q}{\epsilon} N_d x_{n0} = -\frac{q}{\epsilon} N_a x_{p0} \tag{51}$$

which implies that the electric field across the intrinsic region is constant. This is an important property of the p-i-n junction in terms of analyzing charge carrier transport through the intrinsic region [1].

2.6. Electron and Hole Mobility

Understanding the dynamics of charge carriers in semiconductors is important in determining the properties of photovoltaic devices. A famous experiment performed by J. R. Haynes and W. Shockley in 1951 provides a good demonstration of the mobility of electrons in semiconductors under an applied electric field [18]. The basic principle of the experiment includes exciting a number of electrons into the conduction band of a p-doped semiconductor with a pulse of light thus generating a square, narrow pulse of electrons. Under the presence of an external electric field the pulse drifts in a direction opposite to the electric field with a certain drift speed v_d. As the pulse propagates through the semiconductor it also spreads out as the electrons diffuse due to random collisions with atoms in the lattice. The speed with which the square narrow pulse spreads out into a broad gaussian pulse determines the diffusion coefficient D. An important relationship derived from the Haynes-Shockley experiment is

$$v_d = \mu \mathcal{E} \tag{52}$$

where μ is the electron mobility and is constant for a certain material at a fixed

temperature [13, 15, 19]. Therefore, the velocity of a single electron, moving in a lettice with an applied external electric field will *on average* accumulate to $\mu\mathcal{E}$ with a standard deviation proportional to the diffusion coefficient D. Eq. 52 will be used in analyzing the motion of hot carriers.

3.1. Carrier Injection

Solving Eq. 33 for an applied voltage V, without assuming constant equilibrium carrier densities throughout the depleted regions x_{n0} and x_{p0}, Eq. 37 has the following form

$$\frac{p(x_{n0})}{p(-x_{p0})} = \exp\left[\frac{q(V_0 - V)}{k_B T}\right]$$ (53)

Here, an important assumption needs to be made: the majority carrier densities as a function of position in the neutral regions are constant and independent of the applied bias i.e. $p(-x_{p0}) = p_p$. This is a reasonable assumption considering:

1. before the junction was made, the majority carrier densities are taken to be constant with respect to position provided uniform doping, and

2. extra charge carriers provided by the applied bias ionize neutral atoms inside the depletion region which are as uniformly distributed as donor or acceptor ions, which does not affect the charge distribution as a function of distance.

Therefore, for holes, Eqs. 37 and 53 can be combined to obtain

$$\frac{p(x_{n0})}{p_n} = \exp\left(\frac{qV}{k_B T}\right)$$ (54)

According to Eq. 54 there is an exponential increase in minority carrier density on both sides of the depletion region with applied bias. Therefore, the minority carrier

densities on both edges of the depletion region can be expressed as

$$\Delta p_n = p(x_{n0}) - p_n = p_n \exp\left(\frac{qV}{k_B T} - 1\right), \tag{55a}$$

$$\Delta n_p = n(x_{p0}) - n_p = n_p \exp\left(\frac{qV}{k_B T} - 1\right) \tag{55b}$$

The equations for the steady state diffusion current for holes and electrons as a function of x in the n and p sides of the junction respectively are [15]

$$I(x_n) = -qAD_p \frac{d\delta p(x_n)}{dx_n} = qA\frac{D_p}{L_p}\Delta p_n e^{-x_n/L_p}, \tag{56a}$$

$$I(x_p) = -qAD_n \frac{d\delta n(x_p)}{dx_p} = qA\frac{D_n}{L_n}\Delta n_p e^{-x_p/L_n}, \tag{56b}$$

Evaluating Eqs. 56 at $x_n, x_p{=}0$ and combining them with Eqs. 55 an equation for the total current through the junction is obtained

$$I = qA\left(\frac{D_p}{L_p}p_n + \frac{D_n}{L_n}n_p\right)\left[\exp\left(\frac{qV}{k_B T}\right) - 1\right] \tag{57}$$

Eq. 57, also known as the diode equation, was obtained by adding the current due to excess charge carriers on the edge of the depletion region in the p-side of the junction to the negative current due to excess charge carriers on the edge of the depletion region in the n-side of the junction. Since the direction of current is defined as the direction opposite to that of electron flow, the sign of I_n must be reversed [15, 1, 20]. Fig. 12 below shows a typical I-V curve for a p-n junction diode.

3.2. The p-n Junction Under Illumination

In equilibrium there should be no current through the junction, which is what Eq. 57 implies for $V{=}0$. The drift current is canceled by the diffusion current. However, when light shines on a p-n junction in equilibrium electrons are excited on
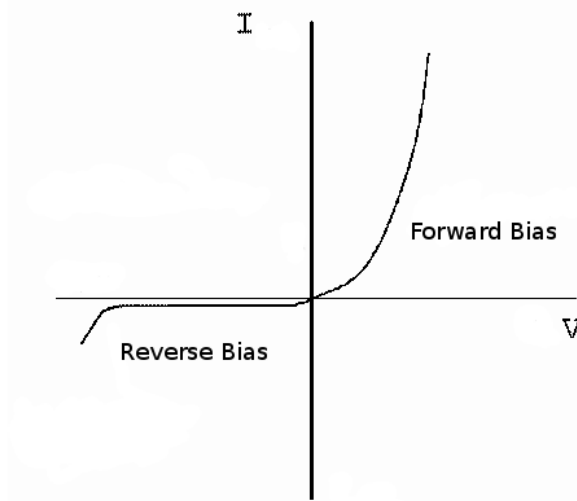
Figure 12. *The ideal diode: An I-V curve for a p-n junction diode showing the exponential increase in the current with applied forward bias. When the bias is reversed the diffusion current is eliminated and since the drift current is independent of the magnitude of the bias the current has a small constant negative value until the reverse bias is larger than the contact potential and breakdown is induced [15].* An I-V curve for a *p-n* junction diode showing the exponential increase in the current with applied forward bias

the edge of the depletion region in the *p*-side and holes are excited on the edge of the depletion region in the *n*-side which are swept across the junction by the built-in electric field. Hence, illuminating a *p-n* junction increases the drift current, but has a negligible effect on the diffusion current. As a result the current in a solar cell under illumination flows in a direction opposite to that of a *p-n* junction under forward bias.

The excited carriers that contribute to the increase in short-circuit current under illumination are only those that can make it to the depletion region before they have lost their excess energy. Therefore, only carriers excited within a diffusion length L_n or L_p are utilized. Since both electrons and holes contribute to the total generation current, the term added to Eq. 57 has the following form
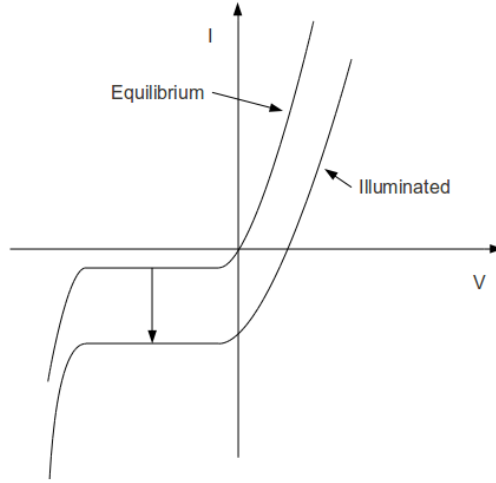
$$I_g = qA\beta(L_p + L_n) \tag{58}$$

28

Figure 13. *An I-V curve for a p-n junction solar cell under illumination: A voltage potential ($\approx V_{oc}$) has to be applied in a direction opposite to that of the voltage potential created by the illuminated device in order to bring the device back to equilibrium ($I = 0$) [15, 6].*

where β is the rate at which electron-hole pairs are excited. Eq.57 take the form

$$I = qA\left(\frac{D_p}{L_p}p_n + \frac{D_n}{L_n}n_p\right)\left[\exp\left(\frac{qV}{k_BT}\right) - 1\right] - qA\beta(L_p + L_n) \qquad (59)$$

Solving Eq. 59 for V in the case of $I = 0$ an expression for the open-circuit voltage V_{oc} is obtained

$$V_{oc} = \frac{k_BT}{q}\ln\left[\frac{L_p + L_n}{(L_p/\tau_p)p_n + (L_n/\tau_n)n_p} \times \beta + 1\right] \qquad (60)$$

The appearance of an open-circuit voltage across a *p-n* junction under illumination according to Eq. 60 is known as the photovoltaic effect. Fig. 14 below illustrates schematically the mechanism of the photovoltaic effect. Fig. 14 b) shows that the generated open-circuit voltage across the photovoltaic junction is the difference in the quasi-Fermi levels. As explained in Sec. 2 applying a forward bias across a *p-n* junction results in a shift in the quasi-Fermi levels that is equal to qV_f. In a
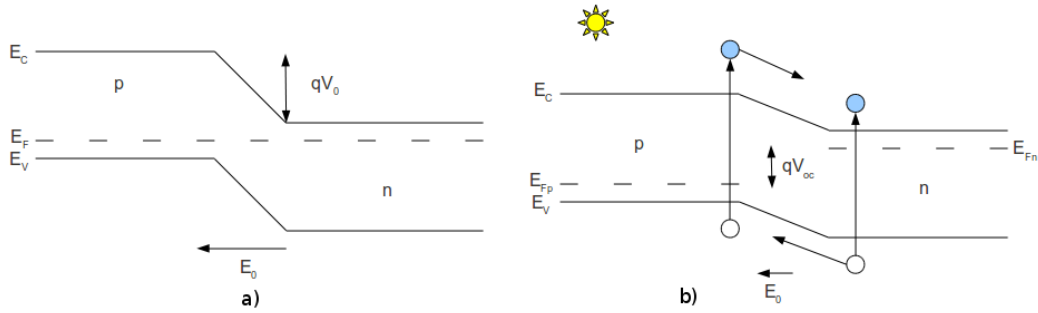
Figure 14. *The effect of illumination: A p-n junction in equilibrium (a) and under illumination (b). Photoexcited carreirs within a diffusion length of the depletion region are swept by the electric field.*

similar manner when a photovoltaic p-n junction is illuminated the quasi-Fermi level for electrons on the n-side is shifted up and the quasi-Fermi level for holes on the p-side is shifted down. The resulting difference in the two energy levels is directly proportional to the open-circuit voltage of the cell according to $qV_{oc} = E_{F_n} - E_{F_p}$ [17, 16].

Electrons can be excited from the valance band into the conduction band by photons of energy $h\nu$ matching or exceeding the bandgap energy E_b. In the case of $h\nu > E_b$ the excited electron possesses energy higher than that of the lattice and is referred to as a *hot* electron. However, hot electrons quickly exchange their energy with the lattice through electron-phonon interaction and thermal equilibrium is achieved on very short time scales depending on the energy of the hot electron and the type of lattice, but usually on the order of picoseconds. Harvesting hot electrons in a photovoltaic device is therefore a matter of collecting the hot electrons before they have thermalized to the bottom of the conduction band. Since the diffusion length of hot electrons is on the order of nanometers, this can be done with absorbers of thickness on the order of nanometers. As pointed out before, Kempa *et al.* have provided experimental verification of the hot electron effect in a photovoltaic device with an extremely thin absorber [7].

4.1. Quantization of Radiation

Maxwell's equations for electromagnetic radiation are suitable for explaining the behavior of light in vacuum, but they fall short of explaining the interaction between light and matter. More specifically, in an attempt to derive the equilibrium distribution of electromagnetic radiation in a hollow cavity (the blackbody radiation spectrum), Maxwell's equation give a good approximation of the distribution for small frequencies only. Rayleigh-Jeans law, which relates the intensity of the electromagnetic radiation inside a hollow cavity to its frequency is derived directly from Maxwell's equations and has the following form:

$$U(\nu)d\nu \sim k_B T \nu^2 d\nu \qquad \text{(Rayleigh-Jeans law)} \qquad (61)$$

where $U(\nu)$ is the intensity as a function of frequency, k_B is the Boltzmann constant and T is the temperature. According to the Rayleigh-Jeans law, the intensity is directly proportional to the square of the frequency, which as shown below in Fig. 15 is a good approximation for small frequencies only.
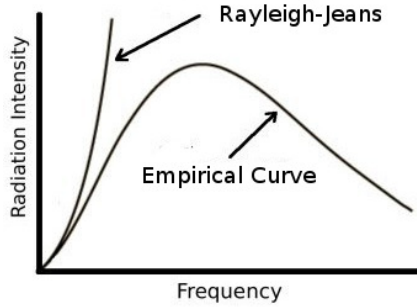

Figure 15. *The Rayleigh-Jeans law vs empirical curve: Agreement with experimental results is seen for small frequencies only [21].*

The source of error in the derivation of the Rayleigh-Jeans law was later shown to come from their assumption that the average energy of an oscillator (a vibrating atom in the walls of the cavity) is $k_B T$ i.e. the energy is a continuous function of the temperature. In order to correct the model, Max Planck made the assumption that the energy of an oscillator is quantized in units of $h\nu$. Since the radiation inside the cavity was in equilibrium with the oscillating molecules in the walls of the cavity, the energy absorbed or emitted by the molecular oscillators was quantized according to $E = nh\nu$. With this correction, Planck arrived at a model which fit the energy distribution curve much better

$$U(\nu) \sim h\nu^3 \frac{1}{e^{h\nu/k_B T} - 1} \tag{62}$$

Therefore, the energy of light can be expressed as the energy of a single quantized unit (photon), which only depends on the frequency of the oscillating electric and

magnetic fields, according to $E = h\nu$, times the number of those quantized units.[21]

4.2. Electron Excitation

A direct proof of Planck's hypothesis is the photoelectric effect. Experimental results showed that when a material in vacuum is irradiated by a beam of light of high enough frequency electrons are ejected from the surface of the material. Moreover, the kinetic energy of the ejected electrons is related to the energy of the light irradiating the material according to

$$K = h\nu - \phi \tag{63}$$

where K is the maximum kinetic energy with which electrons leave the surface of the material and ϕ is the minimum energy needed to just free the electron from the material without giving it any additional kinetic energy (work function). Increasing the intensity of the light does not affect the kinetic energy of the ejected electrons as shown by Eq. 63, but only increases the number of electrons emitted. Thus, it was shown that there is an interaction between a material oscillator (electron) and an electromagnetic oscillator (photon) in which the electron absorbs the photon and is excited to a higher energy level $E_i + h\nu$ where E_i is the electron's initial energy and $h\nu$ is the photon's energy [21]. If a photon is absorbed by an atom on the surface of the material and the photon's energy is higher than the work function of the material, the electron will be freed from the bind of the nucleus and ejected into vacuum. However, if the energy of the absorbed photon is lower than the material's work function, then the eletcron's energy after absorption will not be sufficient enough for it to escape from the attractive forces of the nucleus and the electron will simply be excited to a higher energy level.

4.3. Thermalization

In semiconductors, the Fermi level does not lie in an allowed energy band but in the forbidden gap between the valence band and the conduction band. Therefore, at $0°$ K all energy states in the valence band are occupied and all energy states in the conduction band are empty. In this case, if an electron is excited into a higher energy state it can only jump to the conduction band. However, for such a transition to take place, the electron must absorb energy $E_{absorbed} \geq E_b$. If the excitation is optical, then the photon's energy must be $\hbar\omega \geq E_b$. In the case of $\hbar\omega = E_b$ the electron is excited to the lowest possible state in the conduction band (E_c) and in the case of $\hbar\omega > E_b$ the electron is excited to an energy state above E_c. Fig. 16 below illustrates the two cases.
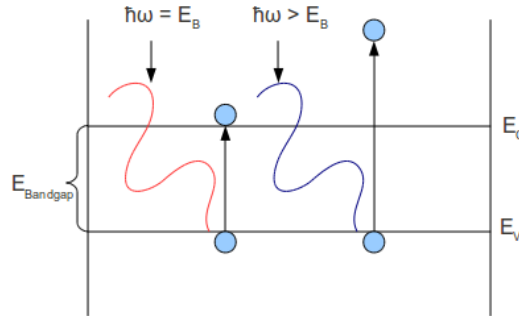

Figure 16. *Band diagram of an absorber with band gap $E_c - E_v$: An electron excited by a photon of energy $\hbar\omega = E_b$ is excited to the bottom of the conduction band and an electron excited by a photon of energy $\hbar\omega > E_b$ is excited to an energy state above the lowest energy state of the conduction band [21].*

The extra energy that the excited electron has in relation to the bottom of the conduction band is $\hbar\omega - E_b$ and the extra energy that the excited electron has in relation to the lattice is $\hbar\omega$. According to the second law of thermodynamics, the electron must come to thermal equilibrium with the lattice over time. In the case of an electron excited to an energy state above the bottom of the conduction band this

process occurs in two steps - thermalization and recombination. Thermalization is the process of the electron losing the energy $\hbar\omega - E_b$ which happens on the time scale of picoseconds [3] and recombination is the process of the electron losing the rest of its energy - E_b which happens on the time scale of tens of microseconds [4, 7]. Since the time scales are so vastly different, in a p-i-n junction where, as described in Sec. 2, the electric field as a function of distance can be considered to be constant, the distance an excited electron drifts while thermalizing is orders of magnitude shorter. In general, the thermalization length is on the order of nanometers and the recombination length is on the order of tens to hundreds of micrometers [22]. Therefore, only the electrons excited within a few nanometers of the n-region are actually collected at an energy higher than E_b.

4.4. Effect on Performance

Conventional solar cells absorption occurs in the vicinity of a p-n junctions where one of the doped materials acts as the absorber. Charge carriers excited near the p-n junction diffuse towards the depletion region while at the bottom of the conduction band and those that make it to the depletion region before recombining are collected as current. In this case the thickness of the absorbing region is orders of magnitude bigger than the thermalization length of electrons. Therefore the performance of the device is determined only by carriers with energy E_b [20].

In order to experimentally detect the hot electron effect in photovoltaic devices the latest research efforts have been extended towards experimenting with devices having absorber thicknesses smaller than the thermalization length of electrons. Theoretically, under such conditions the increase in open-circuit voltage due to hot electron collection should be detectable due to the increase in the ratio of hot-to-cold electrons. The research team of Kempa *et al.* report experimental evidence for the hot electron effect in ultra-thin absorber photovoltaic junctions after they subjected

the device to illumination by high intensity red and blue light and recorded the response. Fig. 4 shows the increase in open-circuit voltage as the cell is illuminated by light of higher frequency. Furthermore, the team have obtained experimental data in proof of the strong dependencassumption1e of the increase in open-circuit voltage on the absorber thickness. Fig. 17 below shows the change in open-circuit voltage ΔV_{oc} resulting from illumination by light sources of different frequency for five different ultra-thin absorber devices of different absorber thickness.
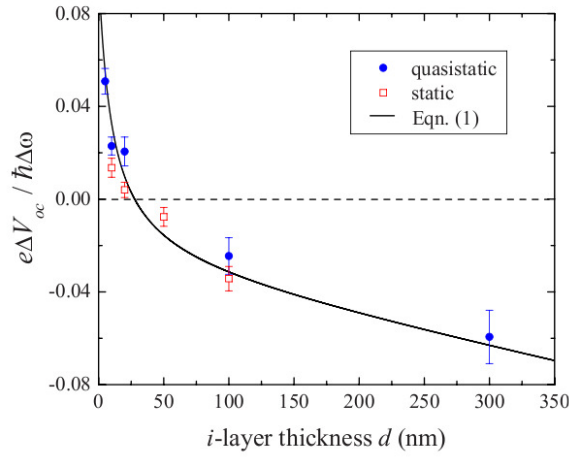

Figure 17. *Curve fit according to Eq. 64: Data points for ΔV_{oc} as a function of absorber thickness d corresponding to samples of d=5, 10, 20, 100, 300 nm, along with a curve fit [7].*

The function fitted to the data points has the following form:

$$\frac{q\Delta V_{oc}}{\hbar\Delta\omega} = \frac{D_c}{D} + \alpha + \beta D \qquad (64)$$

where $\Delta\omega$ is the difference in the energies of two absorbed photons of arbitrary energies ω_1 and ω_2, D_c is the distance from the collector within which photoexcited carriers are collected with energy $\hbar\omega - E_b$ and D is the total junction thickness $d_{abs}+10$ nm and α and β are constants obtained by the curve fit, which correspond to the values -0.03 and -1.2 $\times 10^{-4}$ nm^{-1} respectively. Eq. 64 is derived based on the following two

36

relations

$$E_{avg} \sim (\hbar\omega - E_g)\frac{D_c}{D} \qquad (65)$$

$$\Delta V_{oc} \sim -\Delta d_{abs} \qquad (66)$$

[7, 23] Eq. 64 can be used to approximate $\Delta V_{oc} \approx [(\hbar\Delta\omega)/q]D_c/D$ which clearly points out the improved open-circuit voltage with decreasing the thickness of the absorber.

The subject of research descirbed in this thesis is entirely based on collecting hot carriers through the means of ultrathin absorbers. However, this is not the only the way to harvest the extra energy of hot carriers. It has been shown that through the means of narrow band, energy selective, intermediate bandpass contacts. Such contacts prevent hot carriers from thermalizing by eliminating their interaction with phonons [24].
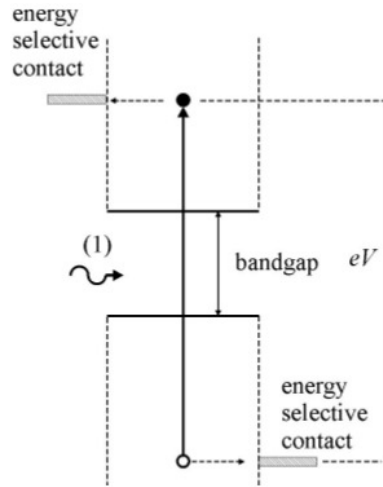

Figure 18. *Isoentropic cooling: Band diagram for hot electron collection through the means of energy selective contacts. The narrow energy band of the selective contact significantly increases the thermalization time for hot carriers collected by those contacts [24]*

Equation 64 provides a good fit for the experimental data obtained, but it is only an empirical relationship derived from simple geometrical consideration ignoring important physical principles. The model assumes that all photoexcited carriers within the region D_c are collected with their maximum kinetic energy which they possess immediately after excitation $\hbar\omega - E_b$. In other words, the model assumes that the energy of a hot carrier as a function of distance is a step function of the following form

$$E(x) = \begin{cases} \hbar\omega - E_b & x < D_c \\ 0 & x > D_c \end{cases}$$

This is a safe assumption for carriers excited within an infinitesimally small distance away from the collector so that they are collected immediately after excitation before they have had time to lose even the smallest quantum of energy. Therefore, from pure thermodynamical considerations, it is reasonable to argue that as long as the absorber has some finite thickness, the collected hot electrons will have energies varying from 0 to $\hbar\omega - E_b$, with $E = 0$ corresponding to the bottom of the conduction band. The model obtained in the publication[7] has the following form

$$\frac{q\Delta V_{oc}}{\hbar\Delta\omega} = \frac{D_c}{d_{abs} + 10\,\text{nm}} + \alpha + \beta(d_{abs} + 10\,\text{nm}) \tag{67}$$

where d_{abs} is the device thickness, D_c is the maximum distance within which all hot carriers are collected with their initial maximum energy $\hbar\omega - E_b$ (i.e. thermalization length), α and β are constants and $(d_{abs} + 10)$ refers to the total device thickness D, with the p-type and the n-type layer each being 5 nm thick. One of the main issues with Eq. 67 is that it is not valid for device thicknesses of $(d_{abs} + 10) < D_c$. Since

thermalization is not accounted for, at absorber thicknesses $d_{abs} < D_c$, the open-circuit voltage as a function of thickness will vary only according to the negative dependence on the temperature. This is not physically relevant since ΔV_{oc} should change with incremental change in d_{abs} when $d_{abs} < D_{oc}$. Fig. 19 below helps illustrate the basic principles behind deriving Eq. 67
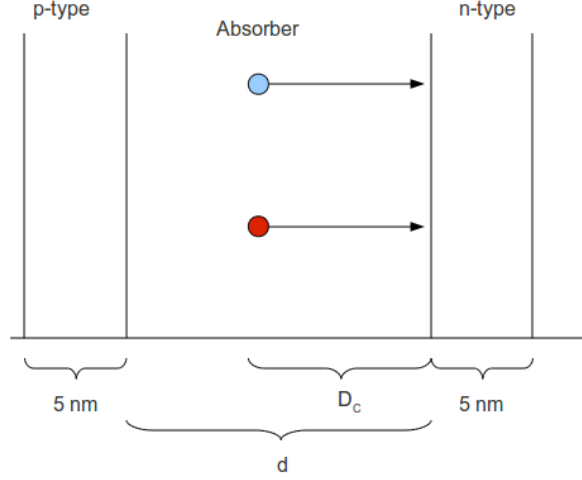

Figure 19. *The model according to Eq. 64: Excited carriers with different initial energies in the conduction band of a p-i-n junction solar cell. The only variable is the absorber thickness d_{abs}.*

Based on the assumptions made in the process of deriving Eq. 67, two electrons excited into the conduction band with different initial energies generate the same ΔV_{oc} regardless of their position, as long as it within distance $x \leq D_c$. However, the excited electrons do thermalize as they travel towards the electrodes. Therefore, for incremental increases Δd_{abs} in the absorber thickness within the interval $0 < d_{abs} < D_c$, $\Delta V_{oc}(d_{abs})$ should decrease not only due to the increase in temperature, but also due to hot electron cooling.

Another major inconsistency of Eq. 67 is that at $d_{abs} = 0$, $q\Delta V_{oc}/\hbar\Delta\omega \neq 1$. By definition $q\Delta V_{oc}$ for two carreirs of different energies is the difference in their energies when collected at the electrode. Therefore as absorber length approaches 0,

the relationship $q\Delta V_{oc} = \hbar\Delta\omega$ should be true and the quantity $q\Delta V_{oc}/\hbar\Delta\omega$ should equal unity at $d_{abs} = 0$, as shown in Fig. 20
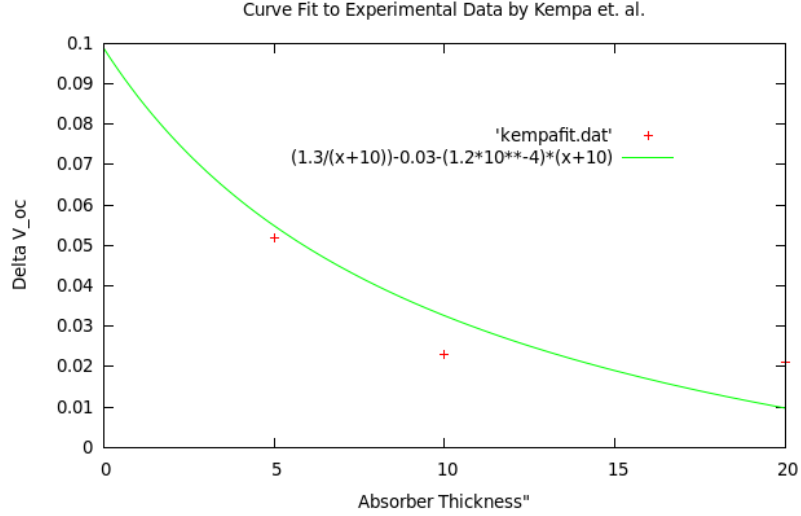

Figure 20. *Fig. 17 zoomed in on the range 0-20 nm: As seen from the graph above,* $q\Delta V_{oc}/\hbar\Delta\omega \neq 1$ *at* $d_{abs} = 0$.

The following theoretical model is centered around accounting for the energy that the hot electrons lose on their way from the point of excitation to the collector. As described in Sec. 4 charge carriers with energy higher than that of the lattice lose their extra energy through thermalization and come in thermal equilibrium with the lattice. This process can be qualitatively described in terms of collisions between the hot electron and 'colder' ones. The goal of the theoretical work described in the following section is to develop a more quantitative model that accounts for the effects of thermalization. The basic principle that underlies the theoretical work is the application of the exponential decay model.

5.1. Assumptions

The model is physically relevant under three major assumptions:

Assumption 1: All photoexcited carriers travel in one preferred direction determined by the junction's electric field and fluctuations in the trajectory due to

collisions with cold atoms is neglected. The motion of hot carriers is ballistic in between collisions and they lose energy instantaneously upon collision.

Assumption 2: All hot electrons lose an equal fraction of their extra energy upon collision, regardless of the amount of energy they possessed immediately before the collision i.e. $E_{before\,collision}/E_{after\,collision} = const$. As a result, the thermalization time for hot carriers is energy independent.

Assumption 3: All photoexcited carreirs, regardless of their initial energy, undergo an equal number of collisions per unit time. This is a reasonable assumption since the lattice spacing is always constant and carriers in the conduction band move with drift velocity approximated by $v_d = \mu \mathcal{E}_0$ where μ and $\mathcal{E}_0$ are constants [13, 19].

5.2. Approach

Since the energy loss rate is directly proportional to the amount of energy the electron possesses, the following relation can be implicated

$$-\frac{dE}{dt} = \gamma E \tag{68}$$

where E is the energy of the carrier traveling through the lattice and γ is a proportionality constant, which is the same for all photoexcited carriers for a fixed temperature. The physical significance of γ in this model is expressed in collisions per unit time and has units of s^{-1}. The solution of this differential equation is

$$E(t) = Ae^{-\gamma t} \tag{69}$$

where the constant A corresponds to the initial value of the energy. Since this model is applied to the motion of the electron within the conduction band immediately

after excitation, $E = 0$ corresponds to the bottom of the conduction band. The constant A corresponds to the initial, maximum energy E_i that the excited charge carrier possess. This energy depends on the energy state that the carrier possesses prior to excitation. Since the model treats the dynamics of a single electron, a choice for that energy level must be made beforehand. For the purpose of simplifying the computational procedure, electrons excited from the top of the valence band will be considered, in which case the maximum energy that they possess immedialety after excitation is

$$E_i = \hbar\omega - E_b \tag{70}$$

To account for an excitation from a lower energy state, Eq. 70 can be corrected with a prefactor a where $0 < a < 1$. Therefore Eq. 69 takes the following form

$$E(t) = (\hbar\omega - E_b)e^{-\gamma t} \tag{71}$$

It is important to note here that hot electrons do not in fact have an infinitely long thermalization time as Eq. 71 predicts. The hot electron is considered to have thermalized when the amount of energy it has left is on the order of the energy of the thermal fluctuations of the lattice atoms. Since a solar cell operates at temperatures higher than $0\ K$, the energies its atoms possess demonstrate a Gaussian distribution centered around $k_B T$ [9]. In the present model a hot electron is considered to have thermalized when its energy is on the order of the energy fluctuation of the lattice.

Using Eq. 52 the time t can be expressed in terms of the distance that the charge carrier has traveled according to $t = x/\mu\mathcal{E}_0$ and therefore an expression for the energy as a function of distance can be obtained

$$E(x) = (\hbar\omega - E_b)\exp\left(-\frac{x\gamma}{\mu\mathcal{E}_0}\right) \tag{72}$$

For hot carriers with different initial energies;

$$E_1(x) = (\hbar\omega_1 - E_b)\exp\left(-\frac{x\gamma}{\mu\mathcal{E}_0}\right) \tag{73a}$$

$$E_2(x) = (\hbar\omega_2 - E_b)\exp\left(-\frac{x\gamma}{\mu\mathcal{E}_0}\right) \tag{73b}$$

the change in open-circuit voltage can be directly related to the difference in the energy between E_1 and E_2. Since $qV_{oc} = E_{F_n} - E_{F_p}$, the gain in open-circuit voltage due to collecting a hot carrier can be attributed to the extra shift in the quasi-Fermi levels. Hot electrons shift E_{F_n} up and hot holes shift E_{F_p} down. The magnitude of that shift can be approximated by Eq. 18 according to which, $E_{tot} \propto E_F$ at room temperatures. The picture below illustrates how two electrons excited by light of different frequency but at equal distances from the collector produce different open-circuit voltages.
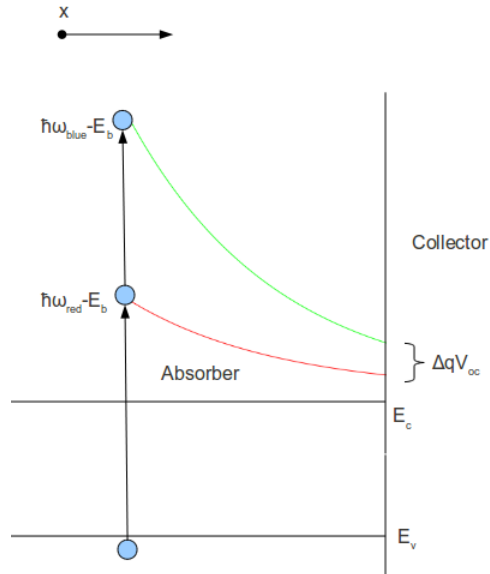

Figure 21. *Exponential decay of hot carriers: Two excited carriers possessing different amounts of initial energy but at equal distances from the collector start to exponentially lose their energy as they drift towards the collector. The smaller the absorber layer, the larger ΔV_{oc}.*

Therefore, ΔV_{oc} as a function of absorber thickness d_{abs} takes the following form

$$\frac{q\Delta V_{oc}}{\hbar\Delta\omega} = \exp\left(-\frac{d_{abs}\gamma}{\mu\mathcal{E}_0}\right) \qquad (74)$$

Eq. 74 is a good approximation for small absorber thicknesses since it does not account for the dependence of the open-circuit voltage on temperature. As the absorber thickness increases, the number of electrons which thermalize before they have reached the collector increases. Their extra energy is lost to heating up the lattice, resulting in a higher temperature of the device and lower open-circuit voltage. Since the absorber thickness is linearly proportional to the number of excited carriers which fully thermalize, the relationship between the absorber thickness and temperature can be approximated as linear: $\Delta d_{abs} \sim \Delta T$. On the other hand, the famous Shockley-Read model, Appendix A, suggests a direct negative relationship between the open-circuit voltage and the temperature: $V_{oc} \sim -T$. Considering this negative proportionality, Eq. 74 should be corrected with a linear term with a negative coefficient. However, for absorber thicknesses on the order of the thermalization length the linear term is dominated by the exponential term and can be neglected. Therefore, in order to provide a more physically relevant fit to the data in Fig. 64 a linear term must be added

$$\frac{q\Delta V_{oc}}{\hbar\Delta\omega} = \exp\left(-\frac{d_{abs}\gamma}{\mu\mathcal{E}_0}\right) - Cd_{abs} \qquad (75)$$

where C is a constant determined by the strength of the dependence of the open-circuit voltage on temperature and is a property of the material.

5.3. Extending the Model Beyond a Single Charge Carrier

Eq. 75 considers a pair of electrons excited an equal distance away from the electrode $x = d_{abs}$. This means that the hot carriers taken into consideration travel the entire length of the absorber. In order to improve the model the charge carriers

44

excited at distances $x < d_{abs}$ must also be accounted for. For that purpose the average $\Delta q V_{oc}$ due to hot carriers excited at all incremental distances Δx away from the electrode must be determined. Therefore V_{oc} must be expressed as a function of x:

$$\frac{q\Delta V_{oc}}{\hbar\Delta\omega} = \exp\left(-\frac{x\gamma}{\mu\mathcal{E}_0}\right) - Cx \tag{76}$$

Next, all the contributions by hot carriers excited at all incremental distances Δx away from the electrode must be added. For this purpose, Eq. 76 must be integrated over the entire absorber length.

$$\sum \frac{q\Delta V_{oc}}{\hbar\Delta\omega} = \int_0^{d_{abs}} \left[\exp\left(-\frac{x\gamma}{\mu\mathcal{E}_0}\right) - Cx\right] dx \tag{77}$$

However, the contribution to the increase in the quasi-Fermi levels by multiple hot carriers is not the sum of the extra energies of each hot carrier, but their average extra energy. Therefore, the increase in $q\Delta V_{oc}$ due to multiple carriers as a function of absorber length becomes

$$\frac{q\Delta V_{oc}}{\hbar\Delta\omega} = \frac{1}{d_{abs}} \int_0^{d_{abs}} \left[\exp\left(-\frac{x\gamma}{\mu\mathcal{E}_0}\right) - Cx\right] dx \tag{78}$$

5.4. Application of the Model to Experimental Results

Eq. 78 was fitted to the experimental data obtained by *Kempa et al.*. The values for ω_{red} and ω_{blue} were directly obtained from the publication, the value of the electric field was calculated based on the doping densities and the value for the electron mobility was obtained from literature [19]. Fig. 22 below shows the curve fit. The important modification of the curve fit obtained through Eq. 67 is seen for absorber thicknesses of 5-20 nm. For these thicknesses the original fit should be corrected with a slight decrease in value of ΔV_{oc} as energy lost due to thermalization
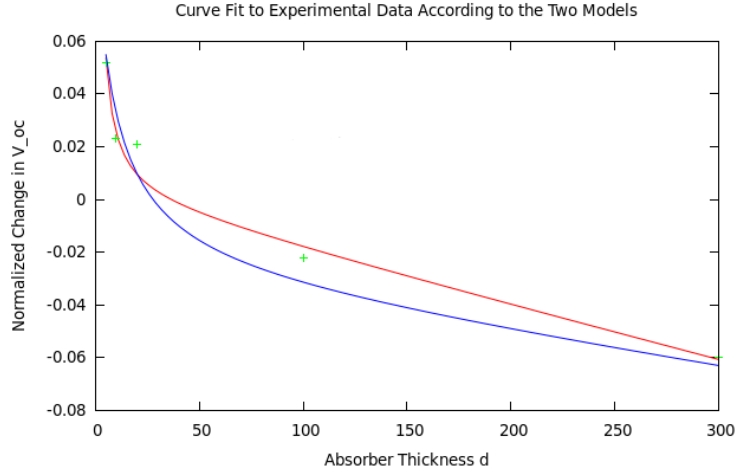
Figure 22. *Curve fit to the data collected by Kempa et al: The red curve is equation 78 fitted to the data points obtained experimentally by Kempa et al. and equation 64 is the blue curve.*

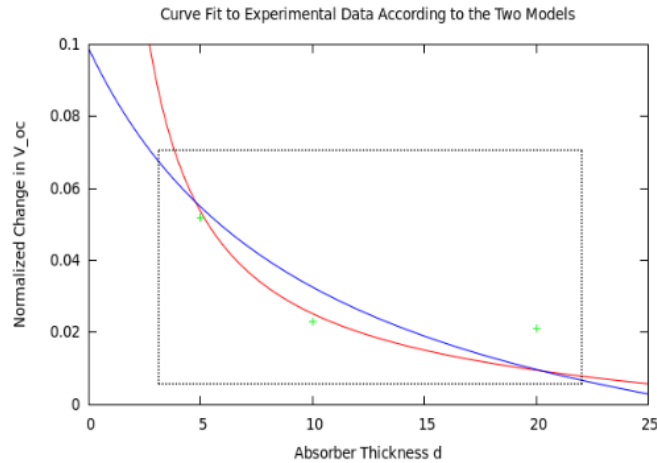is being accounted for. Fig. 23 shows the two models for the range 5-20 nm.

Figure 23. *Fig. 22 zoomed in on the range 5-20 nm: As seen from the graph above Eq. 78 does account for the extra loss in ΔV_{oc} due to hot electron cooling.*

The discrepancy between the two models for very thin absorbers (d_{abs} <5 nm) comes from the fact that Eq. 67 does not take into account the hot carriers' energy loss with change in distance Δd_{abs}.

The value for the thermalization rate γ obtained from the curve fit is $1.2 \times 10^{10} \pm 0.3$ s^{-1}. Substituting this value in Eq. 68 the approximate thermalization rate of

46

hot electrons for the particular device built by Kempa *et al.* can be modeled.
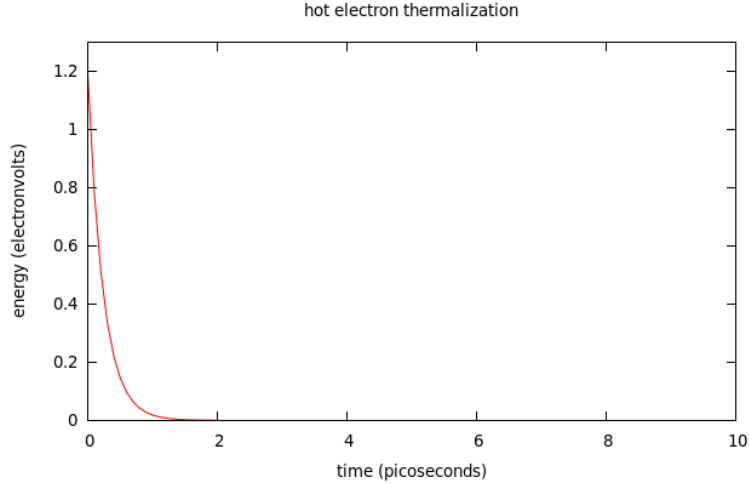

Figure 24. *Thermalization rate: Approximate energy loss rate for a hot electron in the device reported by Kempa et al. An excited carrier loses its energy in approximately 1.3 ps, which corresponds to reported thermalization times for hot electrons in Silicon [25].*

5.5. Discussion

In their publication *Goldman and Prybyla* report that at lower energies the cooling rate is also lower, which adds validity to the assumption that $-dE/dt = \gamma E$ [25]. This, however is only an approximation of the general shape of the curve describing $E(t)$. The excited charged carriers are treated as classical particles which undergo totally elastic collisions with the colder, stationary electrons of the lattice. The value of γ obtained by applying a curve fit to the reported experimental results can be compared to the computed value of γ. Knowing the doping densities, the reported value for the electron mobility in a:Si and the lattice spacing γ can be computed through the following relation

$$\gamma = v_d \rho \tag{79}$$

where ρ is the density of lattice points upon which the hot carrier could undergo a collision. v_d can be obtained through Eq. 52 where $\mathcal{E}$ can be calculated based on the doping densities. Using the doping densities reported in the publication and the value of lattice spacing for a:Si at T=300 K, γ can be approximated to 2×10^{10} s^{-1}, which is in good agreement with the value for γ obtained in Sec. 5.

CHAPTER 6. EXPERIMENT

The nature of the experimental part of the research consists of evaluating the feasibility of semiconducting materials, other than a:Si, forming a p-n junction, as opposed to a p-i-n, junction in the fabrication of ultra-thin photovoltaic devices. CdTe has excellent absorbing properties and is naturally p-type and CdS is naturally n-type. Therefore, the active part of the device is a p-n junction with the CdTe layer acting as the absorber. The goal of the experiment is to approximate the $E(t)$ curve (Fig. 24) for hot electrons in this type of junction and determine the relationship between the gain in open-circuit voltage and the absorber thickness (Fig. 17). For that purpose, multiple devices with varying absorber thicknesses were deposited.

6.1. Material Selection

The properties of the materials involved in hot electron research must satisfy a long list of conditions. The materials for the experimental work described in the following few paragraphs were selected based on their bandgap energy, absorption coefficient, dopability, quantum efficiency.

6.1.1. Absorber

The main criteria according to which the material for the absorber was selected was the bandgap energy E_b. The desired range for the value of E_b is 1.2 - 2 eV, which allows even red photons to excite carriers above the lowest energy state of the conduction band and photons of higher energy to excite carriers to energy states well above the bottom of the conduction band. Therefore, for a small-bandgap material illuminated by red and blue light, the change in open-circuit voltage will be more prominent. CdTe has a bandgap of 1.44 eV, which corresponds to the deep-red part of the visible spectrum and makes it a suitable candidate material. Also, CdTe is naturally p-doped with hole density of approximately $N_a = 1 \times 10^{15}$ cm^{-3} [26, 27].

6.1.2. Window Layer

The window layer must be selected so that it can form an optimal p-n junction with the absorber. High-efficiency CdS/CdTe thin-film solar cells have been extensively reported, which was the main reason for using CdS as the window layer. It has a bandgap of 2.42 eV and doping density of $N_d = 1 \times 10^{17}$ cm^{-3} [28]

6.1.3. Contacts

Since CdTe has high electron affinity of $\chi = 4.4$ eV, it requires a metal with work function of $\phi_m \approx 4.4 + 1.44 \approx 5.84$ eV in order to make an ohmic contact. No metal has such high work function, however there are methods to decrease the rectifying characteristics and increase the ohmic characteristics of the semiconductor-metal junction. One of the most popular and well-documented methods of connecting an electrode to CdTe is adding Cu impurities to the CdTe material and depositing Au as the actual electrode. The Cu layer between the CdTe layer and the Au contact lowers the potential barrier between the metal and the semiconductor and gives the junction ohmic properties [29]. CdS, unlike CdTe, forms ohmic contacts with a wide range of materials. This enables the implementation of a material with an absorption coefficient lower than that of Au. In this case, the device would naturally be oriented so that light enters the cell through the low absorption coefficient contact to minimize losses. The material of choice is Indium Tin Oxide (In$_2$O$_3$:SnO$_2$). With an absorption coefficient of less than 0.1 in the visible, an Indium Tin Oxide layer of less than 100 nm thickness transmits approximately 99 % of the visible light [30].

6.2. Sample Preparation

The device was deposited in superstrate configuration on ITO-coated 25×25 mm glass slides. The samples were obtained from SigmaAldrich™ with thickness of the
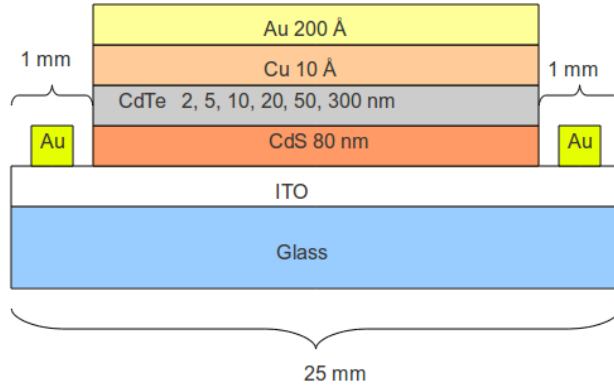
Figure 25. *Cell diagram 1: Cross-section of the device designed for experimentation. The thickness of the CdTe absorber region are varied between 2 and 300 nm.*

ITO coating reported to be 100 nm. Photovoltaic cells with absorber thicknesses of 2, 5, 10, 20, 50, and 300 nm were deposited. Five samples of each cell were prepared. A 10 Å thick layer of Cu was deposited on top of the CdTe layer and the sample was heated for an hour at 180 ℃ so that some of the Cu diffuses into the CdTe in order to form an ohmic back contact. The samples were deposited by RF magnetron sputtering, which is a type of a physical vapor deposition method. Sputtering targets for all of the materials used in fabricating the device were commercially obtained from Kurt J. Lasker™. Figs. 25 and 26 show a diagram of the cell's cross section and a top-down schematic of the photovoltaic device, respectively.

Once the cells were deposited, wires were connected to the front and the back contact so that the leads of a voltmeter or an oscilloscope can be connected to the cell. Since the thicknesses of the contact layers were so small ($\sim$20 nm), soldering the relatively thick wires was disregarded as an option and a more delicate method of making wire contacts was implemented. For that purpose, curable silver ink was used. Silver ink is a substance composed of Ag nanoparticles suspended in thermosetting resin. A drop of the ink was applied to each of the contact layers and a No. 36 AWG wire (0.127 mm in diameter) was embedded into the ink drop. The samples were
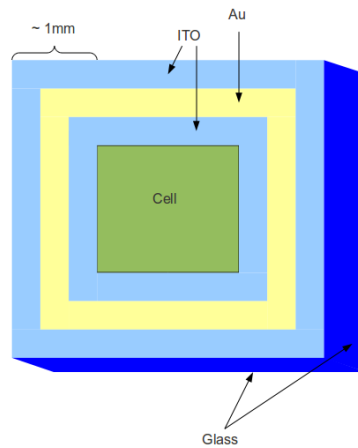
Figure 26. *Cell diagram 2: Top-down view of the cell designed for experimentation. The green square in the middle represents tha active part of the device.*

then cured at 100 ℃ for 45 min. Below is a picture of one of the devices ready for characterization

Figure 27. *Device picture: One of the PVD deposited samples (absorber thickness = 20 nm) ready for characterization.*

6.3. Characterization

Characterization of the deposited devices consisted of testing the samples for the photovoltaic effect and consequently, for the hot electron effect. The tests were

performed with a solar simulator operating under 1.5 artificial suns ($\sim$0.21 W/m^2) using bandpass filters passing narrow spectral band of frequencies in the red and the blue part of the visible spectrum. The sample being characterized was connected to an oscilloscope and the voltage across the leads was monitored as the sample was irradiated.

In order to verify that the results from the solar simulation tests are valid and that the devices were acting as photovoltaic cells, the diode behavior of the samples was tested. As explained in section 3 an ideal p-n junction in the dark has current-voltage (I-V) characteristics similar to Fig. 12. However, the I-V behavior of a photovoltaic device might deviate from that of an ideal p-n junction due to pinholes[31] and resemble that of a resistor. Therefore, I-V curves in the dark for samples 1 through 4 shown in table 1, after annealing, were obtained. The experimental setup consisted of connecting the solar cell in series with a DC supply and an ammeter with known internal resistance. The voltage from the supply was varied from -0.25 to 0.25 V from which the voltage drop across the device was calculated. The magnitude of the current was read directly from the ammeter.

6.4. Experimental Results and Discussion

Out of the samples, only four of the five 300 nm samples demonstrated a photovoltaic response in the solar simulator tests. Table 1 shows the experimental results from the solar simulator tests without the use of optical filters, before and after annealing.

The fact that one of the 300 nm samples showed no photovoltaic behavior and there was an order of magnitude difference in the voltage produced by two of the functioning devices suggested structural inconsistencies and problems using the deposition of the samples.

The I-V curves for samples 1 through 4 from table 1 are shown below.

Sample number	Before heat treatment	After heat treatment
1	no response	no response
2	8.8 mV	38.3 mV
3	6.2 mV	33.2 mV
4	14.8 mV	58.6 mV
5	1.2 mV	5.4 mV

Table 1. Solar simulation test results for the five devices with absorber thickness 300 nm
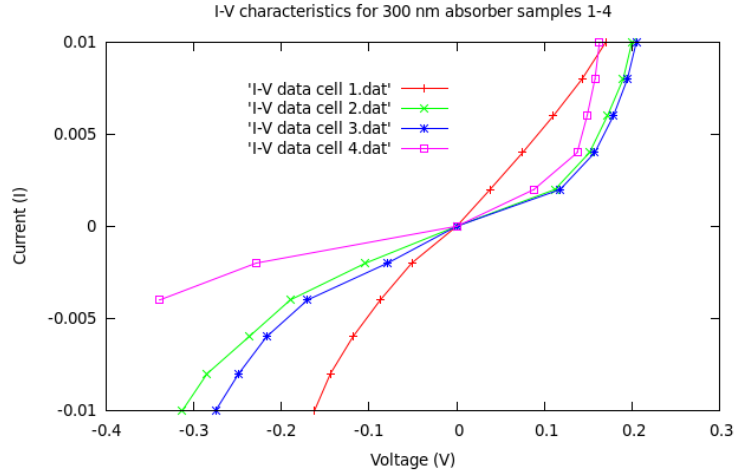

Figure 28. *Device performance: Current-Voltage curves for four of the 300 nm fabricated devices in the dark.*

From the graphs in Fig. 28 it is evident that the less efficient samples (1,2 and 3) have more prominent resistor *I-V* characteristics than the typical *p-n* junction *I-V* characteristics evident in sample 4. Similar results were observed in the samples with smaller absorber thickness. In essence, the majority of the samples exhibited a behavior typical for a resistor, not a photovoltaic device.

In the case of thin film solar cells deposited by the means of physical vapor deposition degradation of performance due to pinholes is a common occurrence [32]. In order to study the structure of the deposited photovoltaic device a scanning electron microscope (SEM) image of the cross section of sample 1 was obtained. The SEM image is shown in Fig. 29.
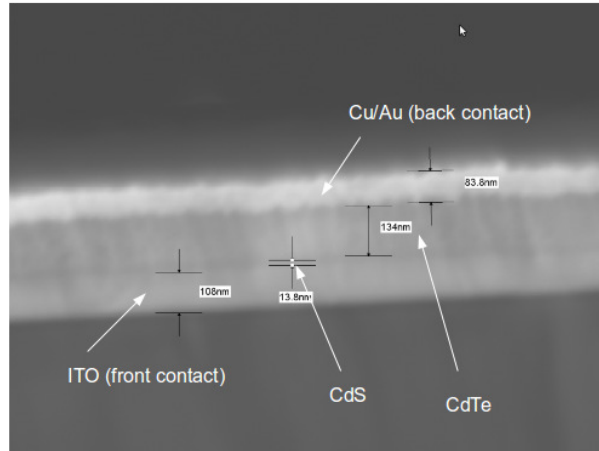
Figure 29. *Spectroscopy analysis: SEM photograph of the cross section of a device with designed absorber thickness of 300 nm. The desired thicknesses of the rest of the layers were those specified in Fig. 25.*

As seen in Fig. 29, there is a significant difference between the desired and actual characteristics of the deposited cells. The 108 nm layer thickness of the ITO layer corresponds to the 100 nm thickness specified by the commercial provider. However, the measured from the SEM photograph thicknesses of the deposited layers are very different from the intended thicknesses. A desired 80 nm thick CdS layer was deposited at a thickness of ∼15 nm and a target 300 nm thick CdTe layer was deposited at a thickness of ∼130 nm. Conversely, the desired combined thickness of the Cu/Au contact of 21 nm was deposited at ∼80 nm. The discrepancy between the desired and the realized thicknesses, however, would not be an issue if the quality of the layers was good, i.e., there was a minimal number of shunting pinholes and the layers were free of impurities. SEM spectroscopy was performed in order to test for the uniformity and chemical composition of the CdS and CdTe layers. The results from the test are shown in Fig. 30.
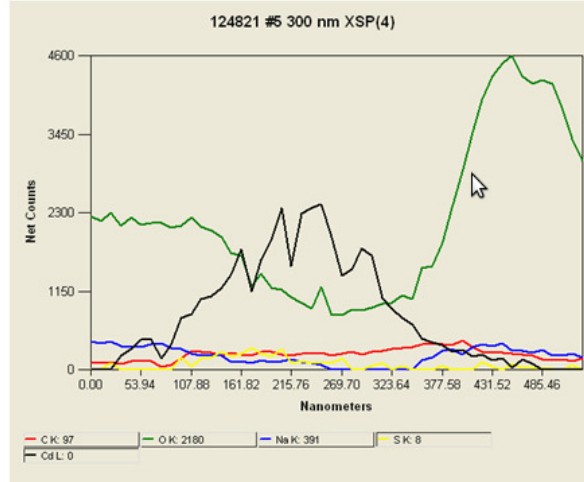
Figure 30. *SEM spectroscopy results for sample 5: The elemental analysis was performed at every point along a thin line across the sample running perpendicular to all the layers. The plot represent the amount of material as a function of distance along that line. The black line corresponds to amount of Cadmium, yellow - Sulfur, blue - Sodium, green - Oxygen, red - Carbon.*

The CdS/CdTe junction spans the 150-to-300 nm portion of the graph in Fig. 30 with the CdS layer corresponding to position values between approximately 150 and 165 nm and the CdTe layer corresponding to position values between approximately 165 and 300 nm. According to the data there is a significant amount of impurities, primarily oxides, in the layers composing the active part of the cell responsible for charge separation. Such a high level of impurities is also known to have degradative effects on CdTe devices [33]. There is also evidence in the figure that the desired composition stoichiometry was not achieved in the Cd-based compounds.

The poor performance of the sample devices can be attributed to multiple factors. First of all, the layers were deposited at thicknesses very different from and well below the desired ones. For example, in the sample analyzed through scanning electron microscopy the deposited absorber layer thickness was three times smaller than the target thickness. If the same relationship between intended and actual thickness is at work for all samples, then the devices with the smallest desired absorber thickness

(2 and 5 nm) would be deposited at thicknesses of approximately tens of angstroms. Devices with absorbers so thin could still in practice be tested for hot electron effect provided that the thin films were deposited with extremely high quality. However, Fig. 28 suggests an abundance of pinholes present in devices with absorbers as thick as 130 nm. Since the probability of a pinhole being formed greatly increases [32] as the films get thinner, it would be quite reasonable to assume that devices with absorber thicknesses on the order of tens of nanometers would exhibit no photovoltaic behavior. This is what was in fact observed in all samples with absorber thickness designed to be less than 300 nm.

CHAPTER 7. CONCLUSION

This thesis summarizes the research efforts extended towards studying the feasibility of utilizing the hot electron effect in an attempt to break the classical Shockley-Queisser limit on solar cell efficiency. This is a relatively new area of research since the first major work on the subject was only published in 2009 . In their publication Kempa *et al.* [7] have provided experimental evidence for the capability of ultra-thin absorber photovoltaic junctions to harvest the extra energy of hot carriers. Their results served as an inspiration to focus the research efforts presented in this thesis on expanding this new area of study. A theoretical model was developed in order to better explain the results obtained by Kempa *et al.* The model accounts for the finite thermalization time of hot electron, which is a physical phenomenon that must be taken into consideration.

Testing the applicability of different materials in a different type of junction suitable for ultra-thin photovoltaic devices that utilize the hot electron effect was the main goal of the experimental work. The experimental efforts were extended towards building a *p-n* junction device in which the *p*-layer would act as the absorber and the *n*-layer as the window. The materials of selection were *p*-type CdTe and *n*-type CdS. The nature of the experiment consisted of building devices with varying absorber layer thicknesses, while keeping the window layer thickness constant. Cells were deposited via physical vapor deposition and characterization methods included solar simulation, scanning electron microscopy and current measurements in the dark. The solar simulation results yielded evidence for photovoltaic behavior only in the samples having absorber thickness >100 nm. There were two possible conclusion drawn from these results:

1) the quality of the absorber layers of thickness < 100 nm was too poor in order to achieve charge separation.

2) the response of the devices with absorber layers of thickness < 100 nm when illuminated with 1.5 artificial suns is too small to detect with the available equipment.

Finally, SEM analysis of one of the samples showed that the absorber thickness of the fabricated devices was approximately a factor of three smaller than the designed thickness. This result adds weight to the conclusion that the deposition of absorbers with thickness < 100 nm was not up to standards.

CHAPTER 8. FUTURE WORK

Although the behavior of hot carriers has been thoroughly researched both on the theoretical and experimental level in the past, application of hot carriers to photovoltaics is an emerging area of research. The 2009 publication "Hot Electron Effect In Nanoscotextitet. al.pically Thin Photovoltaic Junctions" by Kempa *et al.* shows the first promising results in the efforts to surpass the Shockley-Queisser limit by harvesting the energy of hot electrons by using nanoscopically sized absorbers. However, the ground-breaking work of Kempa *et al.* only provides evidence for the feasibility of the proposed method. No commercial ultra-thin photovoltaic device has been developed yet. In order for that to be achieved, extensive experimental and theoretical work needs to be done. The major problem that must be solved is the quantum efficiency of the ultra-thin cells. Since the thickness of the absorber is much smaller than the optimal thickness for the particular photoelectric material, novel solutions for the design of a practical hot electron solar cell are required. The condition for a maximum photon absorption requires a material that is much thicker than the minority carrier diffusion length. Since the ultra-thin junctions are essentially transparent to the solar radiation, the efficiency of such cells is well below the industrial standards. It is essential to find a way to recycle the photons that are not absorbed. In the conventional cells, a reflector is used to reflect light back to the cell so it can be reabsorbed. Also, various elaborate light trapping schemes are employed where the incident light is obliquely coupled into the material, traversing the film several times [6]. Another option would be to decouple the absorbing film thickness from the device thickness making the latter much bigger than the distance that the carriers have to diffuse. This can be achieved, for example, by parallel multi-junction cell design, by folding the thin absorbing layer in a V-shaped structure, or by depositing the ultra-thin solar cell on a nanostructured substrate [34].

8.1. Future Theoretical Work

Although the theoretical model developed here gives a better fit to the experimental results obtained by Kempa *et al.* than the model developed by the team, there is significant room for improvement. The first step of further developing the model is accounting the motion of charge carriers in anisotropic materials. Since the velocity of a charge carrier depends on its direction of motion through the crystal lattice the rate of energy loss would also be affected. Also, one of the major assumptions made in the theoretical model developed here is that motion of the carriers through drifting overwhelms the motion through diffusion. This could be corrected for by modeling the carrier as a particle moving in a two-dimensional lattice. A charge carrier excited at a random point in the lattice, with a certain initial velocity and velocity vector pointing in a random direction, will be accelerated by an electric field in a preferred direction. As the carrier moves through the lattice, the probability of collision with lattice points can be modeled as constant. As a result a certain distribution of collection times will be obtained with a certain part of that distribution matching the thermalization time for hot carriers. This will result in a negative effect on the performance of hot-electron devices since diffusion only has a retardative effect on hot carrier velocity. Furthermore, since most semiconducting materials are not isotropic in nature, the classical theoretical model developed here should be modified in order to account for the carrier motion in anisotropic media.

Another important contribution to the theoretical model would be accounting for quantum confinement. At absorber layer thicknesses of ∼1 nm, the energy states of a free electron in the absorber can no longer be considered continuous. When the height of the potential barriers at the boundaries of the absorber layer is on the order of the length of the potential well (the absorber thickness) a partial quantum well effect is observed. As a result, a charge carrier in the absorber region is excited

into an energy level that has a certain lifetime. Depending on the distribution of energy levels this might either accelerate or retard the thermalization rate of the excited carrier. However, calculation of the energy levels in a shallow potential well composed of an Avogadro's number of particles is a challenge even for today's most advanced computational methods [8, 16].

8.2. Future Experimental Work

So far, the only ultra-thin hot electron device reported is a *p-i-n* junction composed of *p*-doped, intrinsic and *n*-doped Silicon. Therefore, one of the major areas of future research would be experimenting with *p-n* junctions and also experimenting with different semiconducting materials having a bandgap between approximately 1.5 and 2.5 eV. In addition, since doping levels have an effect on the magnitude of the built-in potential, experimental work targeting the optimum doping levels could also prove fruitful.

As far as further characterization work is concerned, poor quality of deposition for devices with small absorber thickness is only a hypothesis. Inability to obtain data from the cells with absorber thicknesses less than 300 nm in the solar simulation tests could result from the fact that the voltages produced by those devices at such low intensities are too small to detect. On the other hand, laser testing was performed by irradiating the cell with a high-intensity peak power oscillator (HIPPO) laser at 355 nm and a repetition rate of 50 KHz at which rate the pulse is ~12 ns long, which is orders of magnitude shorter than the measured RC constant, $2.6 \pm 0.3 \ \mu s$, of the cells. Therefore, characterization with a continuous source of high intensity light, such as a continuous wave (CW) red or blue laser is a strong subject of interest.

REFERENCES

[1] A. L. Fahrenbruch and R. H. Bube, *Fundamentals of Solar Cells*. Academic Press, 1983.

[2] K. Seeger, *Semiconductor Physics*. Springer-Verlag, 1973.

[3] J. R. Goldman and J. A. Prybyla, "Ultrafast dynamics of laser-excited electron distributions in silicon," *Phys. Rev. Lett.*, vol. 72, pp. 1364–1367, Feb 1994.

[4] K. L. Chopra and S. R. Das, *Thin Film Solar Cells*. Plenum Press, 1983.

[5] W. Shockley and H. J. Queisser, "Detailed balance limit of efficiency of p-n junction solar cells," *Journal of Applied Physics*, vol. 32, pp. 510 –519, mar 1961.

[6] J. C. Chen, *Physics of Solar Energy*. John Wiley and Sons, 2011.

[7] K. Kempa, M. J. Naughton, Z. F. Ren, A. Herczynski, T. Kirkpatrick, J. Rybczynski, and Y. Gao, "Hot electron effect in nanoscopically thin photovoltaic junctions," *Applied Physics Letters*, vol. 95, no. 23, p. 233121, 2009.

[8] D. J. Griffiths, *Introduction to Electrodynamics*. Prentice Hall, second ed., 1989.

[9] K. Huang, *Statistical Mechanics*. John Wiley and Sons, 1987.

[10] K. Stowe, *Statistical Mechanics and Thermodynamics*. John Wiley and Sons, Ltd, 1984.

[11] D. J. Griffiths, *Introduction to Quantum Mechanics*. Prentice Hall, first ed., 1995.

[12] R. E. Hummel, *Electronic Properties of Materials*. Spinger-Verlag, second ed., 1993.

[13] N. W. Ashcroft and D. N. Mermin, *Solid State Physics*. Saunders College, 1976.

[14] S. V. Gaponenko, *Optical Properties of Semiconductor Nanocrystals*. Cambridge University Press, 1998.

[15] B. G. Streetman, *Solid State Electronic Devices*. Prentice-Hall, 1972.

[16] J. Nelson, *The Physics of Solar Cells*. Imperial College Press, 2003.

[17] E. Schiff, "Low-mobility solar cells: a device physics primer with application to amorphous silicon," *Solar Energy Materials and Solar Cells*, vol. 78, no. 14, pp. 567 – 595, 2003.

[18] J. R. Haynes and W. Shockley, "The mobility and life of injected holes and electrons in germanium," *Phys. Rev.*, vol. 81, pp. 835–843, Mar 1951.

[19] A. R. Moore, "Electron and hole drift mobility in amorphous silicon," *Applied Physics Letters*, vol. 31, pp. 762 –764, dec 1977.

[20] S. J. Fonash, *Solar Cell Device Physics*. Academic Press, 1981.

[21] D. Bohm, *Quantum Theory*. Prentice-Hall, 1951.

[22] K. H. Bennemann, "Non-equilibrium physics in solids: Hot-electron relaxation," in *Electron Transport in Nanosystems* (J. Bona and S. Kruchinin, eds.), NATO Science for Peace and Security Series B: Physics and Biophysics, pp. 237–247, Springer Netherlands, 2009.

[23] C. Rauch, G. Strasser, K. Unterrainer, W. Boxleitner, K. Kempa, and E. Gornik, "Ballistic electron transport in vertical biased superlattices," *Physica E: Low-dimensional Systems and Nanostructures*, vol. 2, no. 14, pp. 282 – 286, 1998.

[24] R. T. Ross and A. J. Nozik, "Efficiency of hot-carrier solar energy converters," *Journal of Applied Physics*, vol. 53, no. 5, pp. 3813–3818, 1982.

[25] J. R. Goldman and J. A. Prybyla, "Ultrafast hot-electron dynamics in silicon," *Semiconductor Science and Technology*, vol. 9, no. 5S, p. 694, 1994.

[26] K. K. Chin, "p-doping limit and donor compensation in cdte polycrystalline thin film solar cells," *Solar Energy Materials and Solar Cells*, vol. 94, no. 10, pp. 1627 – 1629, 2010.

[27] U. Reislhner, M. Hdrich, N. Lorenz, H. Metzner, and W. Witthuhn, "Doping profiles in cdte/cds thin film solar cells," *Thin Solid Films*, vol. 515, no. 15, pp. 6175 – 6178, 2007.

[28] A. Morales-Acevedo, "Thin film cds/cdte solar cells: Research perspectives," *Solar Energy*, vol. 80, no. 6, pp. 675 – 681, 2006.

[29] A. Niemegeers and M. Burgelman, "Effects of the au/cdte back contact on iv and cv characteristics of au/cdte/cds/tco solar cells," *Journal of Applied Physics*, vol. 81, no. 6, pp. 2881–2886, 1997.

[30] S. Ray, R. Banerjee, N. Basu, A. K. Batabyal, and A. K. Barua, "Properties of tin doped indium oxide thin films prepared by magnetron sputtering," *Journal of Applied Physics*, vol. 54, pp. 3497 –3501, jun 1983.

[31] O. Kunz, J. Wong, J. Janssens, J. Bauer, O. Breitenstein, and A. Aberle, "Shunting problems due to sub-micron pinholes in evaporated solid-phase crystallised poly-si thin-film solar cells on glass," *Progress in Photovoltaics: Research and Applications*, vol. 17, no. 1, pp. 35–46, 2009.

[32] A. Punnoose, M. Marafi, G. Prabu, and F. El-Akkad, "Cds thin films prepared by rf magnetron sputtering in ar atmosphere," *physica status solidi (a)*, vol. 177, no. 2, pp. 453–458, 2000.

[33] B. E. McCandless and J. R. Sites, *Cadmium Telluride Solar Cells*, pp. 600–641. John Wiley and Sons, Ltd, 2011.

[34] I. Kaiser, K. Ernst, C.-H. Fischer, R. Knenkamp, C. Rost, I. Sieber, and M. Lux-Steiner, "The eta-solar cell with cuins2: A photovoltaic cell concept using an extremely thin absorber (eta)," *Solar Energy Materials and Solar Cells*, vol. 67, no. 14, pp. 89 – 96, 2001.

[35] J. Liang, E. A. Schiff, S. Guha, B. Yan, and J. Yang, "Temperature-dependent open-circuit voltage measurements and light-soaking in hydrogenated amorphous silicon solar cells," *Mater. Res. Soc. Symp. Proc.*, vol. 862, 2005.

APPENDIX A. SHOCKLEY-READ MODEL

The model aims at deriving the relationship between the open-circuit voltage and temperature for a *pin* structured photovoltaic device. The rate equations used are

$$\frac{dn}{dt} = G - b_{dn}nP \tag{A.1}$$

$$\frac{dp}{dt} = G - b_{dp}p(N_d - P) \tag{A.2}$$

where G corresponds to the generation rate, b_{dn} to the capture of electrons by positive defects, b_{dp} to the capture of holes by neutral defects, N_d to the density of donor impurities, and P to the density of holes occupying the defects under illumination. The defects are assumed to be positive under illumination and neutral in the dark. Under the requirement for charge neutrality $p + P = n$ and the assumption that $p >> P >> N_d >>$ the steady state solutions are obtained

$$b_{dp}pN_d = b_{dn}nP = G \tag{A.3}$$

$$n = P = \sqrt{\frac{G}{b_{dn}}} \tag{A.4}$$

$$p = \frac{G}{N_d b_{dn}} \tag{A.5}$$

Substituting n and p into Eqs. 45 the following expressions for the quasi-Fermi levels are obtained

$$E_{F_n} \equiv E_c - \frac{k_B T}{2} \ln\left(\frac{b_{dn} N_c^2}{G}\right) \tag{A.6a}$$

$$E_{F_c} \equiv E_v + k_B T \ln\left(\frac{b_{dp} N_v N_d}{G}\right) \tag{A.6b}$$

Expressing qV_{oc} in terms of the quasi-Fermi energy levels in A.6 via $qV_{oc} = E_{F_n} - E_{F_p}$ the following relation is obtained

$$qV_{oc} = E_g - \frac{k_B T}{2} \ln\left(\frac{b_{dn} N_c^2}{G}\right) - k_B T \ln\left(\frac{b_{dp} N_v N_d}{G}\right) \tag{A.7}$$

Hence, for uniform light intensity and uniform doping densities there is a direct negative relationship between open-circuit voltage and temperature.